arXiv:1606.04920v2 [cond-mat.stat-mech] 27 Jan 2017

Particle models with self sustained current

M. Colangeli [*], A. De Masi[†], E. Presutti [‡]

January 30, 2017

Abstract

We present some computer simulations run on a stochastic CA (cellular automaton). The CA simulates a gas of particles which are in a channel, the interval $[1, L]$ in $\mathbb{Z}$, but also in "reservoirs" $\mathcal{R}_1$ and $\mathcal{R}_2$. The evolution in the channel simulates a lattice gas with Kawasaki dynamics with attractive Kac interactions; the temperature is chosen smaller than the mean field critical one. There are also exchanges of particles between the channel and the reservoirs and among reservoirs. When the rate of exchanges among reservoirs is in a suitable interval the CA reaches an apparently stationary state with a non zero current; for different choices of the initial condition the current changes sign. We have a quite satisfactory theory of the phenomenon but we miss a full mathematical proof.

Keywords:— Stochastic cellular automata, Kac potential, Fourier law and phase transition.

1 Introduction

In this paper we introduce models of macroscopic dissipative systems made of interacting particles which move stochastically in a circuit and exhibit a very surprising behavior. Despite the fact that there is no external bias we see, after a transient, an apparently stationary state with a non zero current, with suitably different initial conditions we may select another state with the opposite value of the current. We speculate that on much longer times there is a "dynamical phase transition" with the two states alternating one after the other. To make an analogy with equilibrium phase transitions, consider the 2D Ising model in a large but finite box with nearest neighbor ferromagnetic interactions. Running the Glauber dynamics at a temperature below the critical value we typically see long time intervals where the magnetization density has approximately the plus equilibrium value alternating via tunneling with those where it is close to the minus equilibrium value. The analogue of the equilibrium magnetization in our model is the current as we have two states with opposite values of the current. However we observe our circuit for

[*]Università degli Studi dell'Aquila, Via Vetoio, 67100 L'Aquila, Italy.
E-mail: matteo.colangeli1@univaq.it
[†]Università degli Studi dell'Aquila, Via Vetoio, 67100 L'Aquila, Italy.
E-mail: anna.demasi@univaq.it
[‡]Gran Sasso Science Institute, Viale F. Crispi 7, 00167 L' Aquila, Italy.
E-mail: errico.presutti@gmail.com

times long but much smaller than those for tunneling so that we only see one of the two currents (selected by the initial condition) which then looks stationary. Our analysis relies mostly on computer simulations, we have theoretical explanations but we miss a mathematical proof.

There is a huge literature on the more general question of existence of periodic motions or oscillations especially in the context of biological systems and chemical reactions, the classical reference is the book by Kuramoto, [11]. We just quote here a few examples selected with the purpose of introducing what we will be doing in this paper.

In [15] P. Tass discusses a simple system of rotators which interact attractively with each other and are subject to white noise forces. For small interactions the stationary state is homogeneous and even though each particle rotates there is no macroscopic change. However if the interaction increases the rotators form a macroscopic cluster which then moves periodically. This is a simplified model for neural activities, the angle of the rotator is related to the neuron potential and the crossing from 2π to 0 is interpreted as the neuron discharging its potential ("firing"): the appearance of a cluster causes a great potential change when the cluster crosses 2π which could explain some diseases related to anomalous neuron firing.

A quantum analogue of the rotator model has been studied by Wilczek in [16] where it is shown that there are ground states with a localized cluster which rotates, this phenomenon called a "time crystal". Comments on time crystals can be found in [1]. Experimental evidence of "time crystals" are presented in [18]. Time crystals in a classical (i.e. non quantum) context have been considered in [17].

A rotators model is also considered in [9] where an additional external force is present. The main point in the paper is to show that for a critical set of values of the parameters there is a cluster which is however blocked (by the external force). However if the white noise strength is increased then the cluster starts moving and performs a periodic motion, this being a nice example of noise-induced periodicity. Also in our models noise is the fuel which makes the system run.

In the above models each particle by itself rotates: the macroscopic rotations arise from a "phase synchronization" of the rotators. Instead in the FitzHugh Nagumo class of models for the firing cycles of a neuron, the appearance of periodic motions is due to a different, more intrinsic mechanism. For what follows it is convenient to consider a particular model in the class which can and will be read in a statistical mechanics language. In such a context the model is defined by two (macroscopic) variables, the magnetization m and the magnetic field h. m is the "fast" and h the "slow variable" as the evolution is defined by the equations:

$$\epsilon \frac{dm}{dt} = -m + \tanh\{\beta(m+h)\}, \quad \frac{dh}{dt} = -m \tag{1.1}$$

where $\epsilon > 0$ is the "small parameter" and $\beta > 1$ the inverse temperature. It can be seen that (1.1) has a (stable) periodic solution which in the limit $\epsilon \to 0$ becomes the hysteresis cycle: $m = m_{\pm}(h)$, $m_+(h)$ the positive solution of $m = \tanh\{\beta(m+h)\}$ which exists for $h > -h_c$, $h_c > 0$; $m_-(h) = -m_+(-h)$, $h < h_c$, see Fig. 1. The transition from the upper curve $m_+(\cdot)$ to the lower one $m_-(\cdot)$ (and viceversa) is discontinuous and hence very sharp for $\epsilon > 0$ small, a fact which catches the main feature of the neuron voltage cycle namely that at the firing the potential changes very abruptly. Observe that $m_+(h)$ is metastable for $h < 0$ as well as $m_-(h)$ for $h > 0$, the metastable values of the magnetization will play

a fundamental role also in this paper.

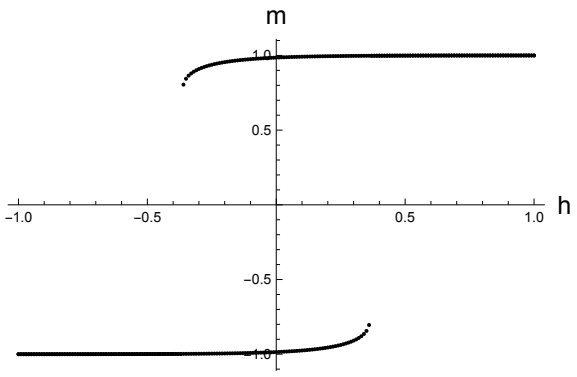

Figure 1: Hysteresis cycle, with $\beta = 2.5$.

Dai Pra et al., [4], derived similar patterns in a macroscopic limit from a Ising spin model with mean field interactions giving nice examples of "intrinsic" periodic oscillations in the stochastic Ising model. In this paper we will consider the relaxed version of mean field as defined by Kac potentials.

All the above examples can be interpreted in terms of a current in a circuit but in all of them there is a more or less hidden bias because the current can flow only in one direction and not in the opposite one, so that they do not fit in what we are looking for. However they have all a common feature with our models, namely the presence of a phase transition, responsible in the rotator models for the formation of a cluster and in the FitzHugh Nagumo models for the presence of a hysteresis cycle. The way phase transitions appear in our analysis is the following. In a first order phase transition there is a spontaneous separation of phases which gives rise to gradients of the order parameter without currents being present. The Fourier law associates to a gradient a current (in the opposite direction) so that the phase transition generates "effective forces" which prevent the gradients to give rise to currents. Our idea is to exploit such forces to construct a "battery" which allows for a non zero current in a circuit.

Our battery is a cellular automaton which simulates the Kawasaki dynamics in a lattice gas with interactions given by an attractive Kac potential which in the Lebowitz-Penrose limit has a van der Waals phase transition. Therefore we can distinguish between stable, metastable and unstable values of the density. The main and somehow unexpected feature of the system is that if we connect the endpoints of the channel to "infinite" (i.e. true) reservoirs which fix the density at values ρ_- and $\rho_+ = 1 - \rho_- > \rho_-$ with $\rho_\pm$ metastable densities we observe numerically a current which goes through the channel from the reservoir with smaller density ρ_- to the one with the larger density ρ_+. We have a theoretical explanation of the phenomenon in terms of properties of the solution of an integral equation obtained from the process in the "mesoscopic limit" where the scaling parameter γ of the Kac potential vanishes, but we could verify these properties only numerically.

In [3] we have presented numerical evidence that the current in the CA flows from the reservoir with smaller density to the one with larger density. In this paper we present a more complete set of simulations from where a very complex structure emerges for which we have a theoretical explanation, but we miss a complete mathematical proof. The other main point in this paper is that we can exploit the above to construct a circuit with a

self sustained current without an external bias, as claimed in the first sentence of this Introduction. This is obtained by making the reservoirs finite and allowing also particles exchanges among the reservoirs. We show (via the simulations) that for suitable values of the parameters there are initial conditions which give rise to a steady non zero current (stationary for the times of our simulations); there are also other initial conditions where the current flows in the opposite direction and still others where there is no current at all. The state with zero current seems unstable while those with a non zero current seem locally stable.

As suggested by a referee, similar phenomena have also been studied in other models, e.g. the Bunimovich's mushroom billiard model [2] in which the presence of peculiar transport regimes can be traced back to the lack of ergodicity of the microscopic dynamics; but we have not yet explored this issue.

The paper is organized as follows. In Section 2 we define two different versions of the CA used in the simulations, namely: one describing a single (open) channel in contact with two reservoirs (hereafter called OS-CA), and another mimicking the particle dynamics in a closed circuit (called CC-CA).
In Section 3 we present the results of the simulations obtained by running the OS-CA and also explain how to run the CC-CA by exploiting the results first obtained with the OS-CA.
In Section 4 we illustrate the behavior of the particle current in the CC-CA and comment on the dependence of this quantity on the parameters of the model.
In Section 5 we study the continuum (mesoscopic) limits of both the OS-CA and the CC-CA, which are described by an integro-differential equation; proofs are deferred to the Appendix B.
In Section 6 we discuss the adiabatic limit of the model, and check the consistency of our simulations of the CC-CA with the predicted adiabatic behavior.
In Section 7 we consider the case where the reservoirs have stable densities and in Section 8 where the densities are not stable.
In Section 9 we study the stability of a stationary density profile, referred to below as *the "bump" solution*, close to the boundary.
Concluding remarks are finally drawn in Section 10.

2 The cellular automata

In this section we define two cellular automata: the first one, called "open system cellular automaton", OS-CA in short, has been first introduced in [12] and then used in [3] to simulate a system in contact with reservoirs. The second one, simply called "closed circuit cellular automaton", CC-CA, is a modification of the first one obtained by making finite the reservoirs and adding direct exchanges between them, so that it simulates a closed circuit.

The OS-CA. The OS-CA describes the evolution of particles in a "channel" $\{1, 2, .., L\}$, $L > 1$ a positive integer. Besides moving in the channel particles may also leave from or enter into the channel through L and 1 (we then say that they are absorbed or released from the reservoir $\mathcal{R}_2$ if this happens at L and from reservoir $\mathcal{R}_1$ if it happens at 1). The two reservoirs are "infinite" in the sense that they do not have memory of the particles

which are absorbed or released.

The CA in the channel is a parallel updating version of a weakly asymmetric simple exclusion process, designed for computer simulations. The $d = 1$ symmetric simple exclusion process is a system of random walks jumping to the right and left with equal probability, the jump being suppressed if the arrival site is occupied. The weak asymmetry that we add is a small bias to jump in the direction where the density is higher. If the channel was a torus this would produce a phase separation into a region where the density is higher and another where it is smaller. But our channel is open as particles may leave or enter into the channel in a setup typical of the Fourier law but in a context where phase transitions are present.

Let us now go back to the definition of the CA. The phase space is $\mathcal{S} = \{(x, v), x \in \{1, .., L\}, v \in \{-1, 1\}\}$, particles configurations are functions $\eta : \mathcal{S} \to \{0, 1\}$, $\eta(x, v) \in \{0, 1\}$ denotes the occupation variable at (x, v) and v will be interpreted as a velocity. $\eta(x) = \eta(x, -1) + \eta(x, 1) \in \{0, 1, 2\}$ denotes the total number of particles at x. We may add a suffix t when the occupation variables are computed at time t.

The definition of the OS-CA involves four more parameters: $\gamma^{-1} \in \mathbb{N}$, $C > 0$ and $\rho_\pm \in [0, 1]$. In the simulations presented in this paper we have fixed $\gamma^{-1} = 30$, $C = 1.25$, while the length of the channel is set equal to $L = 600$. $\rho_\pm$ are referred to as the density of reservoir $\mathcal{R}_2$, respectively $\mathcal{R}_1$, they are fixed during a simulation but they may be changed in different simulations. In the definition of the CA we will use the notation

$$N_{+,x,\gamma} = \sum_{y=x+1}^{x+\gamma^{-1}} \eta^{(+)}(y),\ N_{-,x,\gamma} = \sum_{y=x-\gamma^{-1}}^{x-1} \eta^{(-)}(y), \quad x \in [1, L] \tag{2.1}$$

where $\eta^{(+)}(y) = \eta(y)$ if $y \in [1, L]$ and $\eta^{(+)}(y) = 2\rho_+$ if $y > L$; similarly $\eta^{(-)}(y) = \eta(y)$ if $y \in [1, L]$ and $\eta^{(-)}(y) = 2\rho_-$ if $y < 1$. We want $N_{+,x,\gamma}$ to be the total number of particles to the right of x within distance γ^{-1} from x, however it may happen that if x is close to the right boundary then there are not γ^{-1} sites in the channel to the right of x. Suppose that there are only $\gamma^{-1} - m$ such sites, we then add fictitiously $2m$ phase points (y, v), $v = \pm 1$ and y takes m values to be thought as m physical sites to the right of the channel. The occupation number $\eta(y, v)$ is then set equal to ρ_+ so that the contribution to $N_{+,x,\gamma}$ of the extra m sites is $2\rho_+ m$, which explains the factor 2 in the definition of $\eta^{(+)}(y)$. Analogous interpretation applies to $\eta^{(-)}(y)$.

We are now ready to define how the OS-CA operates: the unit time step updating (from t to $t + 1$) is obtained as the result of three successive operations, we denote by η the configuration at time t, by η' and η'' two consecutive updates starting from η and by η''' the final update which gives the configuration at time $t + 1$.

1. *velocity flip.* At all sites $x \in \{1, .., L\}$ where there is only one particle we update its velocity to become $+1$ with probability $\frac{1}{2} + \epsilon_{x,\gamma}$ and -1 with probability $\frac{1}{2} - \epsilon_{x,\gamma}$, $\epsilon_{x,\gamma} = C\gamma^2[N_{+,x,\gamma} - N_{-,x,\gamma}]$ (the definition is well posed because $(2\gamma^{-1})C\gamma^2 = 2.5/30 < \frac{1}{2}$, $(2\gamma^{-1})$ being an upper bound for $|N_{+,x,\gamma} - N_{-,x,\gamma}|$). At all other sites the occupation numbers are left unchanged. We denote by η' the occupation numbers after the flip.

2. *advection.* After deleting the particles in the channel at $(1, -1)$ and $(L, 1)$ (if present) we let each one of the remaining particles in the channel move by one lattice step

in the direction of its velocity. We denote by η'' the occupation numbers after this advection step.

3. *exchanges with the reservoirs.* With probability ρ_+ we put a particle at $(L,-1)$ and with probability $1-\rho_+$ we leave $(L,-1)$ empty. We do independently the same operations at $(1,1)$ but with ρ_- instead of ρ_+. The final configuration is then denoted by η'''.

The CC-CA. We now turn to the second CA which describes the evolution of particles in a "closed circuit". The phase space is the disjoint union $\mathcal{S}\cup\mathcal{R}_1\cup\mathcal{R}_2$, where $\mathcal{S}$ is as before while the two reservoirs $\mathcal{R}_1$ and $\mathcal{R}_2$ are finite sets both with cardinality R, R a positive, even integer. R is interpreted as the number of phase points in the reservoir, thus there will be $R/2$ sites with velocity 1 and $R/2$ sites with velocity -1: the velocities in the reservoirs however do not play any role in the evolution, they are used only to have a symmetric description of the channel and the reservoirs. Unlike in the OS-CA now the total number of particles (i.e. those in the channel and in the reservoirs) is constant in time. In the CC-CA the densities $\rho_\pm$ in the two reservoirs are no longer constant but given by $N_{\mathcal{R}_1}/R$ and $N_{\mathcal{R}_2}/R$ where

$$N_{\mathcal{R}_1}=\sum_{(x,v)\in\mathcal{R}_1}\eta(x,v),\quad N_{\mathcal{R}_2}=\sum_{(x,v)\in\mathcal{R}_2}\eta(x,v) \tag{2.2}$$

Accordingly we define $N_{\pm,x,\gamma}$ in the CA as in (2.1) but with $\rho_\pm$ replaced by the instantaneous values $N_{\mathcal{R}_1}/R$ and $N_{\mathcal{R}_2}/R$ of the density in $\mathcal{R}_1$ and $\mathcal{R}_2$. With these notation the first two steps of the evolution in the CA are the same as in the OS-CA. We call again η' and η'' the configurations in the system after the first and the second step, with $\eta''=\eta'=\eta$ in $\mathcal{R}_1\cup\mathcal{R}_2$ (i.e. the occupation numbers in the reservoirs are unchanged in the first two steps). In the third step instead they may change as we are going to see.

3. The new third step, (reservoirs exchanges). Its definition involves a new, suitably small parameter $\gamma p>0$. We first select with uniform probability a phase point $(x_1,v_1)\in\mathcal{R}_1$ and $(x_2,v_2)\in\mathcal{R}_2$: if $\eta(x_1,v_1)=0$ we set $\eta'''(1,1)=0$, if instead $\eta(x_1,v_1)=1$ we set $\eta'''(1,1)=1$. Analogously $\eta'''(L,-1)=0,1$ if $\eta(x_2,v_2)=0,1$. This concludes the definition of η''' in the channel while in the reservoirs $\eta'''=\theta'''$, with θ''' defined as follows. We first define θ' by setting $\theta'(x,v)=\eta(x,v)$ for (x,v) in $\mathcal{R}_1$ with $(x,v)\neq(x_1,v_1)$ and $\theta'(x_1,v_1)=0$. $\theta'(x,v)$ is defined analogously in $\mathcal{R}_2$. $\theta''(x,v)$ is obtained from $\theta'(x,v)$ by adding a particle in the first empty point of $\mathcal{R}_1$ (according to a fixed but arbitrary order) if $\eta'(1,-1)=1$, otherwise $\theta''=\theta'$ in $\mathcal{R}_1$. θ'' is defined analogously in $\mathcal{R}_2$. Finally θ''' is obtained from θ'' in the following way. With probability $1-\gamma p$ we let $\theta'''=\theta''$ while with probability γp we do the following: we choose with uniform probability $(y_1,v_1)\in\mathcal{R}_1$ and $(y_2,v_2)\in\mathcal{R}_2$ and exchange $\theta''(y_1,v_1)$ with $\theta''(y_2,v_2)$. To be well defined we have tacitly supposed that $\gamma p\le 1$, actually $\gamma p\ll 1$ in the simulations.

Heuristically γp is the rate at which particles jump directly from a reservoir to the other. Without the channel these exchanges would eventually make the densities of the two reservoirs equal to each other.

Magnetization variables.

To exploit the symmetries in the system it is convenient to introduce spin variables. We set in the CC-CA:

$$\sigma(x)=\eta(x,1)+\eta(x,-1)-1 \tag{2.3}$$

both in the channel and in the reservoirs. (possibly adding t when the variables are computed at time t). We call $S_{\rm ch} = \sum_{x=1}^{L} \sigma(x)$ the total spin in the channel, thus

$$S_{\rm ch} = N_{\rm ch} - L, \qquad N_{\rm ch} := \sum_{x=1}^{L} \eta(x) \tag{2.4}$$

Recalling (2.2), we define analogously to (2.4)

$$S_{\mathcal{R}_1} = N_{\mathcal{R}_1} - \frac{R}{2}, \quad S_{\mathcal{R}_2} = N_{\mathcal{R}_2} - \frac{R}{2} \tag{2.5}$$

We define also the magnetization density in the two reservoirs

$$m_-^{CC} = \frac{S_{\mathcal{R}_1}}{R/2}, \qquad m_+^{CC} = \frac{S_{\mathcal{R}_2}}{R/2} \tag{2.6}$$

In the OS-CA the magnetization density in the "reservoirs" is

$$m_\pm = 2\rho_\pm - 1 \tag{2.7}$$

Currents. For the OS-CA we define $j_{\mathcal{R}_1\to{\rm ch}}(t)$ and $j_{{\rm ch}\to\mathcal{R}_2}(t)$ as the number of particles which go from $\mathcal{R}_1$ to the channel minus those which go from the channel to $\mathcal{R}_1$ in the time step $t \to t+1$ and respectively, the number of particles which go from the channel to $\mathcal{R}_2$ minus those which go from $\mathcal{R}_2$ to the channel in the time step $t \to t+1$. Thus

$$\begin{aligned} j_{\mathcal{R}_1\to{\rm ch}}(t) &= \eta'''(1,1;t) - \eta'(1,-1;t) \\ j_{{\rm ch}\to\mathcal{R}_2}(t) &= \eta'(L,1;t) - \eta'''(L,-1;t) \end{aligned} \tag{2.8}$$

with η', η'' and η''' the occupation numbers after the three updates which lead from t to $t+1$.

In the CC-CA the currents $j^{CC}_{\mathcal{R}_1\to{\rm ch}}(t)$ and $j^{CC}_{{\rm ch}\to\mathcal{R}_2}(t)$ are defined by the same expression as in (2.8) with the new η's. The current between the reservoirs is defined as the number of particles which go from $\mathcal{R}_2$ to $\mathcal{R}_1$ minus those which go from $\mathcal{R}_1$ to $\mathcal{R}_2$ in the time step $t \to t+1$, thus:

$$j_{\mathcal{R}_2\to\mathcal{R}_1}(t) = -\sum_{(x,v)\in\mathcal{R}_2} [\theta'''(x,v;t) - \theta''(x,v;t)] \tag{2.9}$$

Conservation laws. In the OS-CA we have

$$N_{\rm ch}(t+1) - N_{\rm ch}(t) = j_{\mathcal{R}_1\to{\rm ch}}(t) - j_{{\rm ch}\to\mathcal{R}_2}(t) \tag{2.10}$$

In the CC-CA the analogue of (2.10) holds as well:

$$N_{\mathcal{R}_1}(t+1) - N_{\mathcal{R}_1}(t) = j^{CC}_{\mathcal{R}_2\to\mathcal{R}_1}(t) - j^{CC}_{\mathcal{R}_1\to{\rm ch}}(t) \tag{2.11}$$

with analogous formula for $N_{\mathcal{R}_2}$. As a consequence, in the CC-CA, the total number of particles $N_{\mathcal{R}_1} + N_{\mathcal{R}_1} + N_{\rm ch}$ is conserved as well as the total spin $S_{\mathcal{R}_1} + S_{\mathcal{R}_1} + S_{\rm ch}$.

Initial conditions. In the OS-CA we impose $\rho_+ > \rho_-$, $\rho_+ + \rho_- = 1$. Observe that this implies $m_+ > 0$ and $m_+ + m_- = 0$. Analogously in the CC-CA we initially impose that

$$N_{\mathcal{R}_1} + N_{\mathcal{R}_2} = R, \quad N_{\mathcal{R}_2} > \frac{R}{2} \tag{2.12}$$

The initial state in the channel will be specified in the sequel.

Parameters of the simulations. We conclude the section by recalling the values of the parameters that will be used in the simulations:

$$\gamma^{-1} = 30,\ C = 1.25,\ \beta = 2.5,\ L = 600,\ R = 10^5, \quad R =: \gamma^{-1}a,\ L =: \gamma^{-1}\ell \tag{2.13}$$

3 The OS-CA

In this section we present the simulations obtained by running the OS-CA, recall that this CA has been defined in terms of two fixed densities ρ_+ and ρ_-, $\rho_+ + \rho_- = 1$, which in the magnetization variables, see (2.7), amounts to fix $m_+ > 0$, $m_- = -m_+$. As already mentioned the OS-CA simulates the typical Fourier law experiments therefore the physically most relevant quantity is the stationary current $j(m_+)$: $j = j(m_+)$ plays the role of the equation of state in a non equilibrium context (due to the presence of the reservoirs) and defines the "non equilibrium thermodynamics" of the system.

Thus our first task is to consider the currents in the CA, since the instantaneous currents defined in (2.8) are strongly fluctuating, we take averages:

$$j^T_{\mathcal{R}_1\to\mathrm{ch}} = \frac{1}{T}\sum_{t=0}^{T-1} j_{\mathcal{R}_1\to\mathrm{ch}}(t) \tag{3.1}$$

In general with f^T we will denote the average of f, thus $j^T_{\mathrm{ch}\to\mathcal{R}_2}$ is the averaged current from the channel to $\mathcal{R}_2$.

Strictly speaking stationarity is reached as $T \to \infty$, existence of the limit should follow (almost everywhere) from the Birkhoff theorem. Of course in the simulations we cannot take such a limit and the value of T is chosen empirically in such a way that $j^T_{\mathrm{ch}\to\mathcal{R}_2} \approx j^T_{\mathcal{R}_1\to\mathrm{ch}}$ looks independent of T. The initial condition in the channel is with all phase points empty, we have checked that with other conditions the final current does not change appreciably. The stationarity condition $j^T_{\mathrm{ch}\to\mathcal{R}_2}(m_+) - j^T_{\mathcal{R}_1\to\mathrm{ch}}(m_+) \approx 0$ is also satisfied, typical values are 10^{-8} while the currents have order 10^{-5}. 10^{-8} is also considerably smaller than the a-priori bound

$$|j^T_{\mathcal{R}_1\to\mathrm{ch}} - j^T_{\mathrm{ch}\to\mathcal{R}_2}| \le \frac{2L}{T} = 1.2\cdot 10^{-7}, \text{when } T = 10^{10}$$

The black dots in Fig. 2 are the values of $j^T_{\mathrm{ch}\to\mathcal{R}_2}(m_+)$ in the simulations done with $T = 3\cdot 10^9$ for $m_+ \in (0, m')$ and $m_+ > m'''$ and $T = 10^{10}$ elsewhere. The continuous line in Fig. 2, denoted by $j(m_+)$, is a continuous interpolation of $j^T_{\mathrm{ch}\to\mathcal{R}_2}(m_+)$ which we presume to be a good approximation of simulations done with the other values of m_+, it is therefore the "experimental" value for the non equilibrium equation of state $j = j(m_+)$. The main features in Fig. 2 (where $m' = 0.500$, $m'' = 0.825$, $m''' = 0.912$ and $m^{iv} = 0.985$)) are:

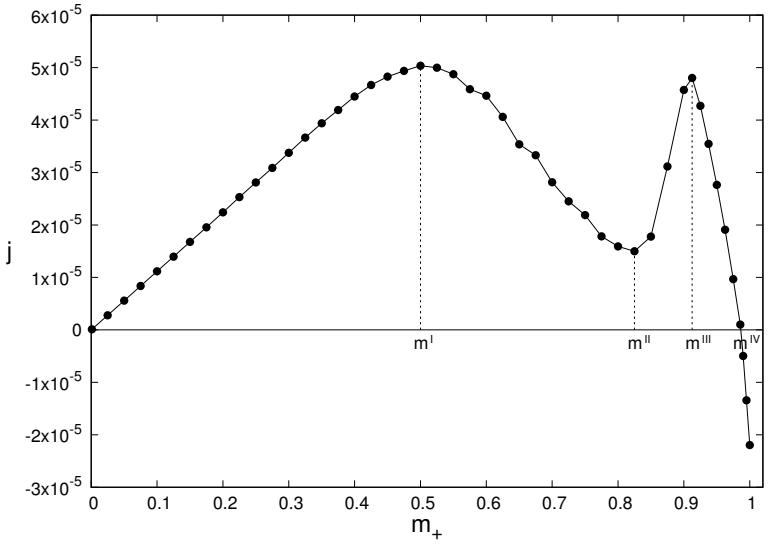

Figure 2: We plot $j := j^T_{\mathrm{ch}\to\mathcal{R}_2}$ as a function of m_+ (black dots). The continuous line is $j(m_+)$. Shown are the values $m' = 0.500$, $m'' = 0.825$, $m''' = 0.912$, $m^{iv} = 0.985$.

- For $m_+ \in (m^{iv}, 1]$ the current $j(m_+)$ is negative in agreement with the Fourier law, while for $m_+ < m^{iv}$ the current is positive going from smaller to larger values of the magnetization (i.e. from m_- to m_+).
- $j(m_+)$ is first increasing till m', then decreasing till m'', again increasing till m''' and finally decreasing then after.
- In Fig. 3 we plot $j^t_{\mathcal{R}_1\to\mathrm{ch}}(m_+)t$ and $j^t_{\mathrm{ch}\to\mathcal{R}_2}(m_+)t$, $t \le T$ with $m_+ \in [m', m''']$. We see significant fluctuations around the linear slope $j^T_{\mathcal{R}_1\to\mathrm{ch}}(m_+)t$, while for $m_+ \notin [m', m''']$ the fluctuations are "negligible".

The most striking feature in the simulations is undoubtedly the fact that the current is positive when $m_+ < m^{iv}$ so that it flows along the gradient going from the reservoir with smaller magnetization to the one with larger magnetization. If we dropped the interaction among particles in the channel, namely put $\epsilon_{x,\gamma} \equiv 0$, then the current would flow according to the Fourier law opposite to the gradient, namely from $\mathcal{R}_2$ to $\mathcal{R}_1$.

A heuristic argument. Let us now imagine to have two channels connected to $\mathcal{R}_1$ and $\mathcal{R}_2$, channel 1 is the channel considered so far while channel 2 is some other channel where the Fourier law is satisfied (for instance the OS-CA with no bias, $\epsilon_{x,\gamma} \equiv 0$, or some simpler connection as the one discussed later). When $m_+ < m^{iv}$, in channel 1 there is a current $j(m_+)$ going from $\mathcal{R}_1$ to $\mathcal{R}_2$, while in channel 2 the current is $j_2 = \kappa m_+$, $\kappa > 0$, going from $\mathcal{R}_2$ to $\mathcal{R}_1$ (recall $m_- = -m_+$). Thus in a time t the reservoir $\mathcal{R}_1$ will loose a magnetization $j(m_+)t$ through channel 1 and gain a magnetization $\kappa m_+ t$ through channel 2; the opposite happens to $\mathcal{R}_2$. This will go forever because the reservoirs in the OS-CA are not changed by what comes and goes; if instead the reservoirs were realized by large but finite systems (as in CC-CA) then after a time which depends on the size of the reservoirs and the difference $j(m_+) - \kappa m_+$ the magnetization in the reservoirs would change and stationarity would be lost. However if we choose channel 2 so that $\kappa m_+ = j(m_+)$ there is a perfect

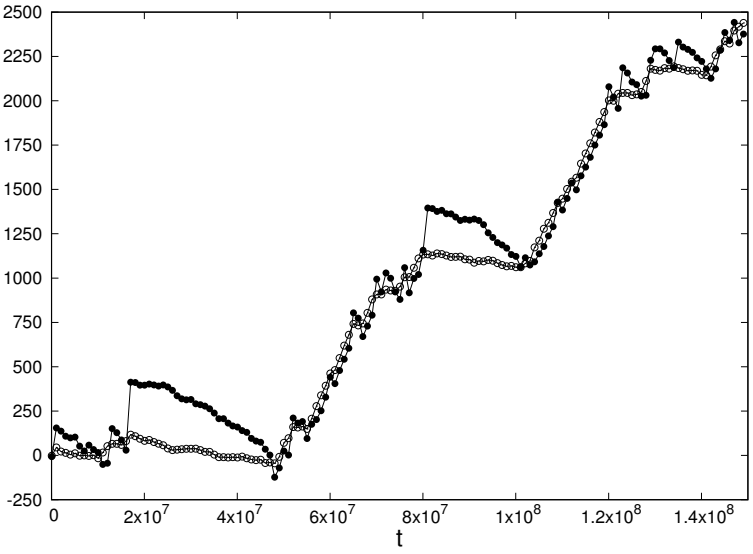

Figure 3: We plot $j^t_{\mathcal{R}_1\to\mathrm{ch}}(m_+)t$ (black circles) and $j^t_{\mathrm{ch}\to\mathcal{R}_2}(m_+)t$ (empty circles) as functions of time t , with $m_+ \in [m', m''']$.

balance so that what $\mathcal{R}_1$ gives to $\mathcal{R}_2$ through channel 1 comes back from channel 2. We may thus hope that even if the reservoirs are finite (yet sufficiently large) this is again approximately true and that there is a non zero current which looks stationary for long times.

The simplest choice for channel 2 leads to the CC-CA of Section 2 where channel 2 is made by just allowing direct exchanges between the two reservoirs. Then, as we shall see later, the average current in the CC-CA from $\mathcal{R}_2$ to $\mathcal{R}_1$ is equal to $\gamma p m_+$, hence the conjecture that for such a particular value of γp there is a non zero stationary current in the circuit which is close to $j(m_+)$.

To check this we have defined for each $m_+ < m^{iv}$ in Fig. 2 $\gamma p = j(m_+)/m_+$ as a function of m_+, see Fig. 4.

We have then run the CC-CA with such values of γp, putting $m_+(0) = m_+$ in $\mathcal{R}_2$, $m_-(0) = -m_+$ in $\mathcal{R}_1$ and choosing the initial state in the channel equal to the configuration in the OS-CA simulation at the final time T. For all the values of m_+ considered in Fig. 2 we have run the CC-CA for a same time $T = 3 \cdot 10^9$ and computed the averaged currents $j^{T,CC}_{\mathcal{R}_1\to\mathrm{ch}}$, $j^{T,CC}_{\mathrm{ch}\to\mathcal{R}_2}$ and $j^{T,CC}_{\mathcal{R}_2\to\mathcal{R}_1}$ defined as in (3.1). Recalling (2.6) we have also defined the averaged magnetization $m^{T,CC}_{\pm}$ in the two reservoirs writing $j^{T,CC}_{\mathcal{R}_2\to\mathcal{R}_1}(m_+), j^{T,CC}_{\mathcal{R}_1\to\mathrm{ch}}(m_+)$, $j^{T,CC}_{\mathrm{ch}\to\mathcal{R}_2}(m_+), m^{T,CC}_{\pm}(m_+)$ when we want to underline that the values are obtained starting from m_+.

The previous heuristic argument suggests that the three currents above are all close to each other and thus approximately equal to $j^T_{\mathrm{ch}\to\mathcal{R}_2}(m_+)$ and moreover that $m^{T,CC}_{\pm}(m_+) \approx \pm m_+$. In the next section we will see what the simulations say.

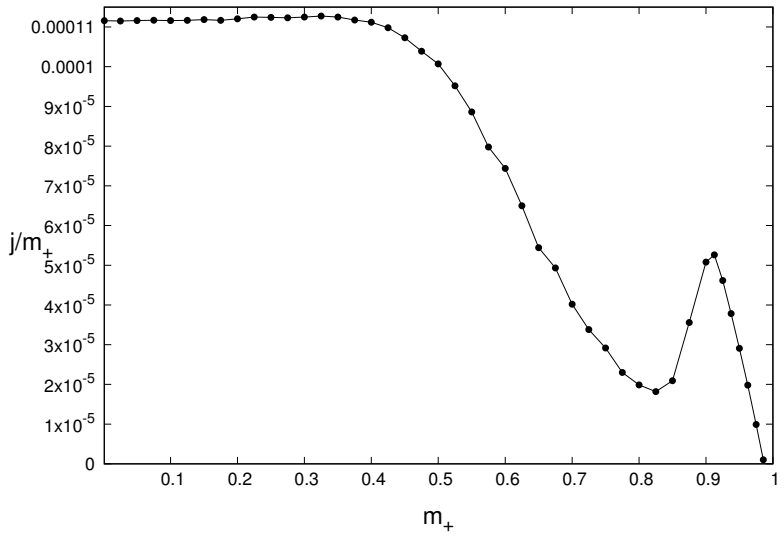

Figure 4: We plot $j/m_+ := j(m_+)/m_+$ as a function of m_+ (black dots). The continuous line is a black dots interpolation.

4 Self sustained currents

Fig. 5 is obtained by running the CC-CA in the setup described at the end of the previous section. It reports the values of the differences $10^5[j^{T,CC}_{\mathcal{R}_2\to\mathcal{R}_1}(m_+) - j^{T,CC}_{\text{ch}\to\mathcal{R}_2}(m_+)]$ and $m^{T,CC}_+(m_+) - m_+$ as a function of m_+, recall from Fig. 2 that the typical values of the current have order 10^{-5}.

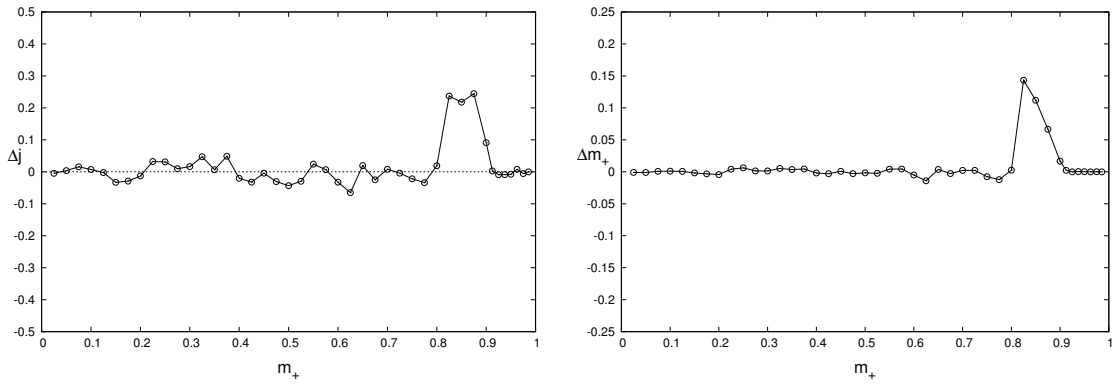

Figure 5: We plot $\Delta j := 10^5 \times [j^{T,CC}_{\mathcal{R}_2\to\mathcal{R}_1}(m_+) - j^{T,CC}_{\text{ch}\to\mathcal{R}_2}(m_+)]$ (left panel) and $\Delta m_+ := m^{T,CC}_+ - m_+$ (right panel) as a function of m_+. Note that the large fluctuations occur in the interval (m'', m'''), with $m'' = 0.825$, $m''' = 0.912$.

We have also reported for each m_+ in Fig. 2 the values of the pair $(\gamma p, j^{T,CC}_{\mathcal{R}_2\to\mathcal{R}_1})$, see Fig. 6 left, the continuous line is obtained by interpolating between such values. Analogously in Fig. 6 right the dots are the values of $(\gamma p, m^{T,CC}_+)$ and the continuous line is obtained by interpolation. The continuous lines are multi-valued functions denoted respectively by $j^{CC}(\gamma p)$ and $m^{CC}_+(\gamma p)$, we presume they are a good approximation of what would be obtained by following the same procedure for other values of m_+ in Fig. 2.

Let us point out the main features of our simulations.

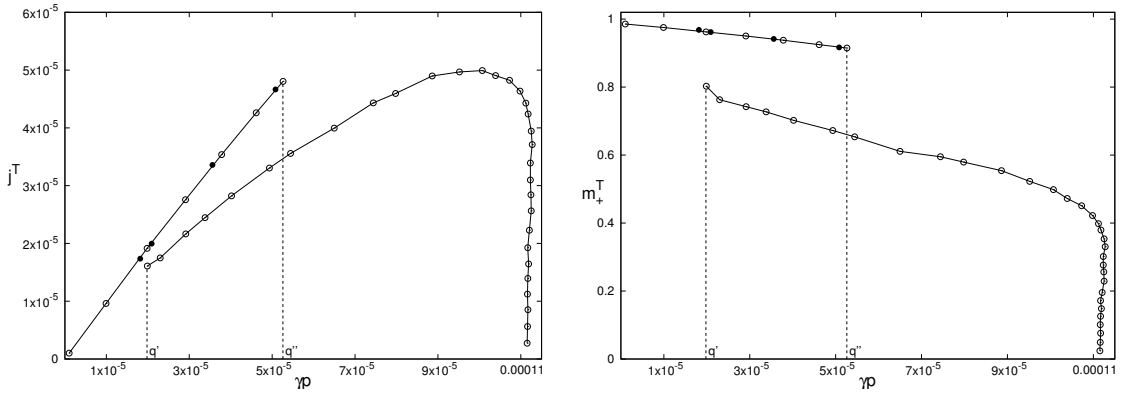

Figure 6: We plot the values of the pairs $(\gamma p, j^T := j^{T,CC}_{\mathcal{R}_2\to\mathcal{R}_1})$ (left panel) and $(\gamma p, m_+^T := m_+^{T,CC})$ (right panel). The black circles in the panels above denote, respectively, the stationary values of $j^{T,CC}_{\mathcal{R}_2\to\mathcal{R}_1}$ and $m_+^{T,CC}$ obtained with $m_+ \in (m'', m''')$. Shown are also the values of $q' = 1.98\times10^{-5}$ and $q'' = 5.26\times10^{-5}$.

- Fig 5 shows that the simulations are in good agreement with the conjectures stated at the end of the previous section except in the interval $m_+ \in (m'', m''')$. The values of $j^{T,CC}_{\mathcal{R}_2\to\mathcal{R}_1}(m_+)$ and $m_+^{T,CC}(m_+)$ when $m_+ \in (m'', m''')$, are however approximately the same as those obtained for different values of m_+, see the black circles in Fig. 6).

- The values of γp are all in the interval $(0, q_c)$, $q_c = 11.25 \times 10^{-5}$, and $j^{CC}(\gamma p)$ is positive for all such values of γp. We have also done simulations with $\gamma p > q_c$ with several choices of the initial condition and we have always seen zero current (not reported here).

- $j^{CC}(\gamma p)$ is multi-valued, it has two distinct branches (separated from each other), the upper one in the interval $(0, q'')$, $q'' = 5.26 \times 10^{-5}$, the lower one in the interval (q', q_c); $q'' > q'$, $q' = 1.98 \times 10^{-5}$. In the interval (q', q'') there are two positive currents different from each other.

- $m_+^{CC}(\gamma p)$ has the analogous structure, being two valued in (q', q''). Both branches are decreasing, $m_+^{CC}(\gamma p) \to m^{iv} = 0.985$, as $\gamma p \to 0$, and to 0 as $\gamma p \to q_c$.

- There is a gap in the range of $m_+^{CC}(\gamma p)$, namely the interval (m', m'').

Conclusions. The simulations in Fig. 5 show good agreement with the conjectures of Section 3 except when $m_+ \in (m'', m''')$. Thus, with such exception, we may say that the stationary state found in the OS-CA evolution persists in the CC-CA provided that $\gamma p = j(m_+)/m_+$.

There is no mystery about the current between the two reservoirs being $\gamma p(m_+ - m_-)/2 \approx \gamma p m_+$ because we can prove (see Appendix A) that

$$E\Big[\{j^{T,CC}_{\mathcal{R}_2\to\mathcal{R}_1} - \gamma p\frac{1}{2}[m_+^{T,CC} - m_-^{T,CC}]\}^2\Big] \le \frac{\gamma p}{T} + 16\frac{(\gamma p)^2}{R} + \text{ corrections} \qquad (4.1)$$

Since $\gamma p \approx 10^{-5}$, $R = 10^5$ and $T \approx 10^9$, the corrections have order 10^{-19}, see (A.18).

Fig. 6 can be obtained from Fig. 2: in fact according to the above statements $j^{CC}(\gamma p)$ is (approximately) equal to $j(m_+)$ with $j(m_+) = \gamma p m_+$. Since this may have multiple roots, $j^{CC}(\gamma p)$ will be correspondingly multi-valued. However the roots with $m_+ \in (m'', m''')$ are absent in the simulations (see the black circles in Fig. 6) but their values are the same as those obtained with other values of m_+. Same if we look at $m^{CC}(\gamma p)$ and compare with Fig. 2.

As a conclusion we have a consistent explanation of what seen in the OS-CA and the CC-CA, but we still need to explain (i) what happens when $m_+ \in (m'', m''')$; (ii) why the typical values of $j(m_+)$ have order 10^{-5} which is much smaller than $1/L \approx 10^{-3}$ which is what expected from Fourier law experiments; (iii) why the true reservoir current has the behavior shown in Fig. 2.

We can gain a theoretical insight on what is going on by looking at what happens in the mesoscopic limit $\gamma \to 0$ which we study in the next section.

5 The mesoscopic limit

This is defined by letting $\gamma \to 0$ with

$$L = \gamma^{-1}\ell, \quad R = \gamma^{-1}a, \quad \ell, a > 0 \text{ fixed} \tag{5.1}$$

In the channel space and time are scaled diffusively, thus $x \to r = \gamma x$ and $t \to \tau = \gamma^2 t$. In mesoscopic units the channel after the limit $\gamma \to 0$ becomes the real interval $[0, \ell]$. We will prove existence of the limit (for the relevant quantities) under the assumption of a strong form of propagation of chaos, the details are given in an appendix.

We denote by E_γ the expectation in the CA processes (randomness coming from the initial datum and from the updating rules of the CA's).

Assumptions. We suppose that

1. In both CA the limit below (denoted in the same way for both CA) exists and is smooth

$$\lim_{\gamma\to 0} \lim_{\gamma x \to r, \gamma^2 t \to \tau} E_\gamma[\eta(x, v, t)] = \frac{m(r, \tau) + 1}{2}, \quad r \in [0, \ell], v \in \{-1, 1\}, \tau \geq 0 \tag{5.2}$$

2. In the CC-CA

$$\lim_{\gamma\to 0, \gamma^2 t \to \tau} m_{\pm,\gamma}(\gamma^2 t) = m_\pm(\tau) \tag{5.3}$$

   where, recalling (2.6), we have set $m_{\pm,\gamma}(\gamma^2 t) := E_\gamma[m^{CC}_\pm(t)]$

3. In both CA for all $r, r_1, r_2 \in (0, \ell)$, $r_1 \neq r_2$, $v \in \{-1, 1\}$ and $\tau \geq 0$

$$\begin{aligned} &\lim_{\gamma\to 0} \lim_{\gamma x \to r, \gamma^2 t \to \tau} |E_\gamma[\eta(x, v, t)\eta(x, -v, t)] - E_\gamma[\eta(x, v, t)]E_\gamma[\eta(x, -v, t)]| = 0 \\ &\lim_{\gamma\to 0} \lim_{\gamma x \to r_1, \gamma y \to r_2, \gamma^2 t \to \tau} |E_\gamma[\eta(x, t)\eta(y, t)] - E_\gamma[\eta(x, t)]E_\gamma[\eta(y, t)]| = 0 \end{aligned} \tag{5.4}$$

4. In the CC-CA for all $\tau \geq 0$

$$\lim_{\gamma \to 0, \gamma^2 t \to \tau} R^{-1} E_\gamma \Big[\big| N_{\mathcal{R}_i}(t) - E_\gamma[N_{\mathcal{R}_i}(t)] \big| \Big] = 0, \quad i = 1, 2 \tag{5.5}$$

In Appendix B we will prove the following two Theorems.

Theorem 1 (Mesoscopic limit)**.** *Under the above assumptions, in both CA, the limit magnetization $m(r,t)$ satisfies:*

$$\frac{\partial}{\partial t} m(r,t) = -\frac{\partial}{\partial r} I(r,t), \quad r \in (0,\ell) \tag{5.6}$$
$$I(r,t) = -\frac{1}{2} \Big\{ \frac{\partial m(r,t)}{\partial r} - 2C[1 - m(r,t)^2] \int_r^{r+1} [m(r+\xi,t) - m(r-\xi,t)] d\xi \Big\}$$

with $m(r+\xi,t) = m_+(t)$ if $r + \xi \geq \ell$ and $m(r-\xi,t) = m_-(t)$ if $r - \xi \leq 0$ in the CC-CA; same expression holds in the OS-CA but with $m_\pm(t)$ replaced by $m_\pm$. Moreover

$$m(0,t) = m_-, \quad m(\ell,t) = m_+, \qquad \text{in the OS-CA} \tag{5.7}$$

while in the CC-CA

$$m(0,t) = m_-(t), \quad m(\ell,t) = m_+(t) \tag{5.8}$$
$$\frac{d}{dt} m_+(t) = \frac{1}{a} \Big(2I(\ell,t) + p[m_-(t) - m_+(t)] \Big) \tag{5.9}$$
$$\frac{d}{dt} m_-(t) = \frac{1}{a} \Big(-2I(0,t) + p[m_+(t) - m_-(t)] \Big) \tag{5.10}$$

A proof which avoids our assumptions of propagation of chaos has been obtained in [10] for a lattice gas with Kac potential and Kawasaki dynamics in a torus. In magnetization variables the system becomes the Ising model with Kac potential and the limit equation is (5.6). In [12] it has been studied the macroscopic scaling limit of this system with space scaled by $\gamma^{-\alpha}$ and time by $\gamma^{-2\alpha}$, $\alpha > 1$ ($\alpha = 1$ is the mesoscopic limit considered above).

Theorem 2 (Currents)**.** *Denote by $j_{x,x+1}(t)$ the number of particles which in the time step $t, t+1$ cross the bond $(x, x+1)$, $x \in \{1, .., L-1\}$ (counting as positive those which jump from x to $x+1$ and as negative those from $x+1$ to x). Then, under the above assumptions, in both CA, for all $r \in (0,\ell)$ and $\tau > 0$*

$$\lim_{\gamma \to 0 : \gamma x \to r} \gamma \sum_{t=0}^{T-1} E_\gamma[j_{x,x+1}(t)] = \int_0^\tau I(r,s) ds, \qquad T = [\gamma^{-2}\tau] \tag{5.11}$$

$$\lim_{\gamma \to 0} \gamma \sum_{t=0}^{T-1} E_\gamma[j_{\mathcal{R}_1 \to \mathrm{ch}}(t)] = -\int_0^\tau I(0,s) ds,$$
$$\lim_{\gamma \to 0} \gamma \sum_{t=0}^{T-1} E_\gamma[j_{\mathrm{ch} \to \mathcal{R}_2}(t)] = \int_0^\tau I(\ell,s) ds \tag{5.12}$$

where $I(r,s)$ is given in (5.6)*.*

In the CC-CA the current between reservoirs converges by (4.1) to:

$$\lim_{\gamma\to 0}\gamma\sum_{t=0}^{T-1}E_\gamma[j_{\mathcal{R}_2\to\mathcal{R}_1}(t)]=\int_0^\tau pm_+(s)ds \tag{5.13}$$

In the simulations we have plotted the quantity $j^T_{\mathrm{ch}\to\mathcal{R}_2}$. This is related by (5.12) to the mesoscopic current I by

$$\begin{aligned}
E_\gamma[j^T_{\mathcal{R}_1\to\mathrm{ch}}]&=\frac{\gamma}{T}\sum_{t=0}^{T-1}E_\gamma[j_{\mathcal{R}_1\to\mathrm{ch}}(t)]\approx-\frac{\gamma}{\tau}\int_0^\tau I(0,s)ds,\\
E_\gamma[j^T_{\mathrm{ch}\to\mathcal{R}_2}]&=\frac{\gamma}{T}\sum_{t=0}^{T-1}E_\gamma[j_{\mathrm{ch}\to\mathcal{R}_2}(t)]\approx\frac{\gamma}{\tau}\int_0^\tau I(\ell,s)ds\\
E_\gamma[j^T_{\mathcal{R}_2\to\mathcal{R}_1}]&=\frac{\gamma}{T}\sum_{t=0}^{T-1}E_\gamma[j_{\mathcal{R}_2\to\mathcal{R}_1}(t)]\approx\frac{\gamma}{\tau}\int_0^\tau pm_+(s)ds
\end{aligned}\tag{5.14}$$

so that the experimental values of the three currents scale all as γ when $\gamma\to 0$.

We next show that there is a natural interpretation of the solutions of the system (5.6)–(5.10) in terms of statistical mechanics, which then allows to relate what seen in the simulations to phase transitions and metastable–unstable magnetization values.

Free energy functional and thermodynamic potentials. The evolution equation (5.6) in $[0,\ell]$ with periodic boundary conditions is the gradient flow relative to a non local free energy functional $F(m)$, in fact

$$\begin{aligned}
&I(r)=-\chi\frac{\partial}{\partial r}\frac{\delta F(m)}{\delta m(r)},\quad \chi=\frac{\beta}{2}(1-m^2),\quad \beta=2C\\
&F(m)=\int\Big(-\frac{m^2}{2}-\frac{S}{\beta}\Big)+\frac{1}{4}\int\int J(r,r')[m(r)-m(r')]^2\\
&S(m)=-\frac{1-m}{2}\log\frac{1-m}{2}-\frac{1+m}{2}\log\frac{1+m}{2}\\
&J(r,r')=1-|r-r'|,\qquad \text{for } |r-r'|\le 1\quad\text{and }=0\quad\text{elsewhere}
\end{aligned}\tag{5.15}$$

$F(m)$ is "the mesoscopic free energy functional", the Ginzburg-Landau functional is a local approximation of $F(m)$ where the non local term becomes a gradient squared. The corresponding gradient flow evolution is the Cahn-Hilliard equation, which can then be viewed as a local approximation of (5.6).

The important point for us is that $F(m)$ specifies the thermodynamics of the system. In fact

$$f_\beta(m)=-\frac{m^2}{2}-\frac{S(m)}{\beta} \tag{5.16}$$

is the van der Waals mean field free energy; its convex envelope $f^{**}_\beta(m)$ is the thermodynamic free energy. $f^{**}_\beta(s)$ is obtained by minimizing $F(m)/\ell$ under the constraint $\int m(r)=\ell s$ and then taking the limit $\ell\to\infty$, see for instance [14], Ch. 6.

The equilibrium magnetization density when there is a magnetic field h is the solution of the mean field equation

$$m=\tanh\{\beta(m+h)\} \tag{5.17}$$

When $\beta > 1$ there is $h_c(\beta) > 0$ so that for any $|h| < h_c(\beta)$, $f_\beta(m,h) = f_\beta(m) - hm$ is a double well function of m. The local minima are $m_+(h)$ and $m_-(h)$ and their graph is the hysteresis cycle, see Fig. 1. In particular at $h = -h_c(\beta)$, $m_+(h) = m^*$

$$m^* > 0 : \beta[1 - (m^*)^2] = 1 \tag{5.18}$$

so that the magnetization in (m^*, m_β) and in $(-m_\beta, -m^*)$ is metastable. At $h = 0$ the double well is symmetric and the local minima are global minima, they are attained at $m = \pm m_\beta$, m_β the positive solution of (5.17) with $h = 0$. $\pm m_\beta$ are the equilibrium magnetization at the phase transition with $h = 0$ and $\beta > 1$. $m_+(h)$ and $m_-(h)$ are the unique equilibrium magnetization at $h > 0$ and respectively $h < 0$.

6 The adiabatic limit.

Some of the characteristic parameters of the simulations are related to the thermodynamics associated to the mesoscopic equations, see the end of Section 5. Indeed in fig 2 which refers to simulations with the OS-CA, the value 0.985 is very close to m_β so that the simulation shows that the current is negative when m_+ is stable, namely $m_+ > m_\beta$ and positive when $m_+ < m_\beta$ (metastable or unstable). Correspondingly when there is a current in the CC-CA then $m_+ < m_\beta$, see fig. 6 right. The above validates the considerations in the Introduction about the relation between the appearance of a current in the circuit and the occurrence of phase transitions.

Also the metastable region (m^*, m_β) has a role in the simulations as the interval (m'', m''') is a subset of (m^*, m_β) (because $m'' = 0.825$ and $m''' = 0.912$ while $m^* \approx 0.775$ and $m_\beta \approx 0.985$); thus the gap phenomenon (i.e. that some values of the magnetization in $\mathcal{R}_2$ are never seen for all γp) occurs only inside the metastable region.

We turn now to the heuristic argument at the end of Section 3 by observing that it becomes rigorous in the context of the mesoscopic equations. In fact if m is a stationary solution of the mesoscopic equation for the OS-CA when the reservoirs magnetizations are $m_\pm$, and the corresponding current I is positive, then $u = m$ in the channel and $u = m_\pm$ in $\mathcal{R}_i$ $i = 1, 2$ is a stationary solution of the CC-CA mesoscopic equations with $p = \frac{I}{\frac{1}{2}(m_+ - m_-)}$, recall that the ratio between the mesoscopic current and the current in the CA scales as γ^{-1}. Thus for sufficiently small γ we may expect to see what conjectured at the end of Section 3.

We can also give an explanation of the gap phenomenon (i.e. that for all γp the magnetization in the reservoirs $\mathcal{R}_2$ is never in the interval (m'', m''')) by assuming that the evolution of the OS-CA is well approximated by the mesoscopic equations in the adiabatic limit that we are going to define. We first observe that the OS-CA can be regarded as the "infinite reservoirs limit" of the CC-CA, in fact in the limit $R \to \infty$ the updating rules of the CC-CA become those of the OS-CA. This is true also at the mesoscopic level: when $a \to \infty$ the magnetizations $m_\pm(t)$ converge to their initial value $m_\pm(0)$ and the evolution becomes that of the OS-CA. The above is true when we let $a \to \infty$ keeping the time finite, more interesting behaviour is seen if we scale time proportionally to a, which is the so called adiabatic scaling limit. Suppose (in agreement with the simulations in fig. 2) that for each value of m_+ (and with $m_- = -m_+$) there is a unique stationary solution of

the mesoscopic equations for the OS-CA, $I_{\rm stat}(m_+)$ being the corresponding current. We then say that the CC-CA mesoscopic equations have a "good adiabatic behavior" if in the adiabatic limit the magnetizations $m_\pm(t)$ satisfy the equations

$$\frac{dm_+(t)}{dt} = 2\Big(I_{\rm stat}(m_+(t)) - pm_+(t))\Big) \qquad m_-(t) = -m_+(t) \tag{6.19}$$

Suppose now that $I_{\rm stat}$ is positive with a graph like $j(m_+)$, see fig. 2. Then the stationary solutions of $pm_+ = I_{\rm stat}(m_+)$ with $m_+ \in (m'', m''')$ are linearly unstable because $I_{\rm stat}(m_+)$ is decreasing while pm_+ is increasing. Thus a small perturbation will lead the magnetization away from the stationary value $pm_+ = I_{\rm stat}(m_+)$, $m_+ \in (m'', m''')$, and presumably it will converge to one of the two other solutions of $pm_+ = I_{\rm stat}(m_+)$. This may therefore explain why in the simulations we do not see the magnetization $m_+ \in (m'', m''')$ and instead find another solution of $pm_+ = I_{\rm stat}(m_+)$.

We can check experimentally whether the CC-CA has a good adiabatic behavior by doing simulations with non stationary initial data. In fig. 7 we report the experimental values and those obtained by solving numerically the adiabatic equations.

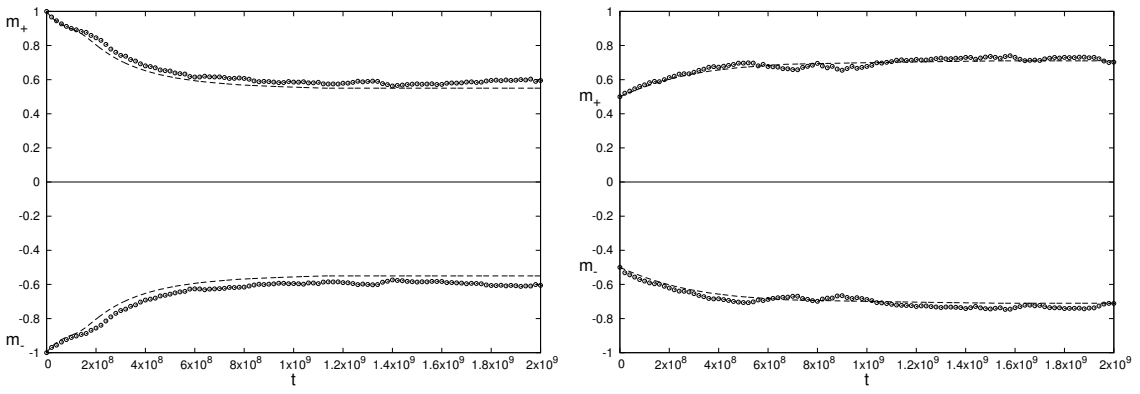

Figure 7: We plot $m_\pm$ as functions of time t (empty circles), obtained by running the CC-CA, as well as the predicted behavior in the adiabatic limit (dashed line). The initial values of the magnetization are, respectively, $m_+(0) = -m_-(0) = 1$ (left panel) and $m_+(0) = -m_-(0) = 0.5$ (right panel).

We do not have an analytic proof of good adiabatic behavior which instead can be rigorously proved for another particle model. This is the simple symmetric exclusion process in an interval with boundary processes at the endpoints which simulate reservoirs with densities $\rho_\pm(t)$ dependent on time. In [6] it is proved that in a scaling limit where $\rho_\pm(t)$ are "slowly varying" the current in the system becomes at each time t the same as the stationary current when the densities at the endpoints are kept fixed at the values $\rho_\pm(t)$.

Summarizing, we have a reasonable explanation of the simulations in the CC-CA once we accept the behavior of the current $j(m_+)$ in the OS-CA as given in Fig. 2. To explain the latter we need to go deeper in the analysis of the simulations discussing the magnetization profile in the channel, which will be the argument of the remaining sections.

7 The instanton and the Stefan problem

We have a good understanding of what happens when $m_+ \in (m_\beta, 1]$. In Fig. 8 we plot the time evolution of the magnetization pattern when $m_+ = 1$, but a similar picture is observed for the other values of $m \in (m_\beta, 1]$. The simulation shows convergence as time increases to a profile which is therefore stationary (in the times of the simulation) and it agrees with what found studying the mesoscopic equations. The existence of stationary solutions $m_{\rm st}(r;\ell;m_\pm)$ of (5.6) with boundary conditions (5.7) when $m_+ > m_\beta$ has been proved in [5] for ℓ large enough. It is also shown that

$$\lim_{\ell\to\infty} m_{\rm st}(r\ell;\ell;m_\pm) = m_{\rm st}(r;m_\pm), \quad r \in (0,1) \tag{7.1}$$

where the limit $m_{\rm st}(r;m_\pm)$ is antisymmetric around $r = 1/2$ and satisfies the equation

$$-\frac{1}{2}[1-\beta(1-m_{\rm st}^2)]\frac{dm_{\rm st}}{dr} = I_{\rm st}(m_+), \quad r \in [\frac{1}{2}, 1] \tag{7.2}$$

where $I_{\rm st}(m_+)$ is determined by requiring that $m_{\rm st}(1/2) = m_\beta$ and $m_{\rm st}(1) = m_+$. For $m_+ = 1$, $\beta = 2.5$ and $m_\beta = 0.985$ from (7.2) we get $I_{\rm st}(1) \simeq -7.2 \times 10^{-3}$. To compare with the simulations we have to divide by $L = \gamma^{-1}\ell = 600$ getting -1.2×10^{-5} the current in the simulations of the cellular automata OS -CA is instead $\simeq -2.2 \times 10^{-5}$. The discrepancy is possibly due to ℓ not being large enough. In [5] it is also proved that

$$\lim_{\ell\to\infty} m_{\rm st}(\frac{1}{2}+x;\ell) = \bar m(x), \quad x \in \mathbb{R} \tag{7.3}$$

where $\bar m(x)$ is the instanton solution of

$$\bar m(x) = \tanh\{J * \bar m(x)\} \tag{7.4}$$

namely the antisymmetric function solution of (7.4) which converges to m_β as $x \to \infty$. See for instance [14] for existence and properties of the instanton.

In Fig. 8 it is also plotted the time evolution of the magnetization pattern when starting away from the stationary one. The approach to the latter occurs on the time scale L^2.

Conjecture. *Let $m(r,t;\ell;m_\pm)$ be the solution of (5.6) with boundary conditions (5.7) and with initial datum $m_0(r\ell)$, $r \in [0,1]$, such that:*

- *$m_0(r) < -m_\beta$ is smooth in $r < r_0$, $r_0 \in (0,1)$ with limits m_- and $-m_\beta$ as $r \to 0$ and $r \to r_0$*
- *$m_0(r) > m_\beta$ is smooth in $r > r_0$, with limits m_β and m_+ as $r \to r_0$ and $r \to 1$.*

Then

$$\lim_{\ell\to\infty} m(r\ell, t\ell^2;\ell) = m(r,t) \tag{7.5}$$

where $m(r,t)$ is the solution of the Stefan problem with initial datum $m_0(r)$:

$$\frac{\partial}{\partial t}m(r,t) = -\frac{\partial}{\partial r}I(r,t), \quad I(r,t) = -\frac{1}{2}[1-\beta(1-m(r,t)^2)]\frac{\partial}{\partial r}m(r,t) \tag{7.6}$$

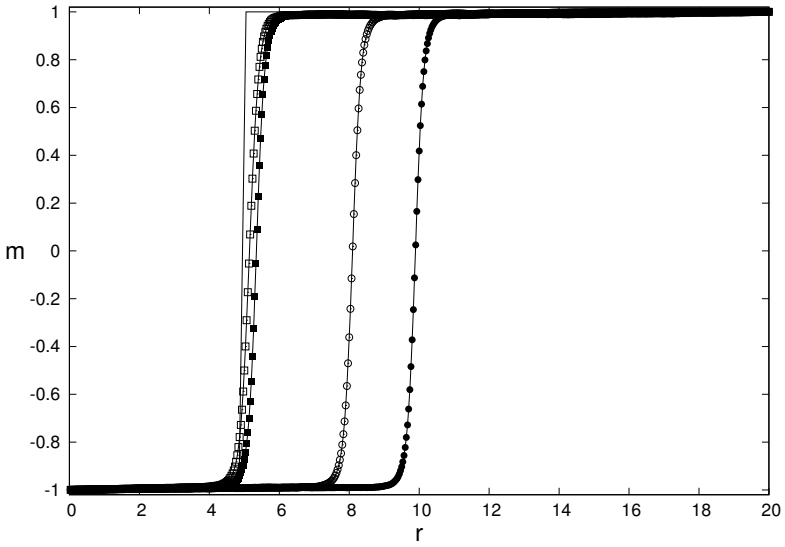

Figure 8: Magnetization profile with $m_+ = 1$. The different curves in the plot correspond to the averaged magnetization computed at different times: $t = 10^5$ (empty squares), $t = 10^6$ (black squares), $t = 10^7$ (empty circles) and $t = 10^8$ (black circles). The black thin line denotes the initial configuration, corresponding to a step function centered at $r = 5$.

where (7.6) *holds in* $\{r < r_t\}$ *and in* $\{r > r_t\}$ *with Dirichlet boundary conditions* m_- *and* $-m_\beta$ *in* $\{r < r_t\}$ *and* m_β *and* m_+ *in* $\{r > r_t\}$. *The free boundary* r_t *is also an unknown and it is determined by* (7.6) *and the condition*

$$2m_\beta \frac{dr_t}{dt} = I(r_t^-, t) - I(r_t^+, t) \tag{7.7}$$

We do not have a proof that $m(r,t) \to m_{\rm st}(r; m_\pm)$ as $t \to \infty$ ($m_{\rm st}(r; m_\pm)$ as in (7.1)). However if the pattern looks like the one in Fig. 8, i.e. essentially linear away from $\pm m_\beta$, then the current (being proportionally to the slope) when $r > r_t > 1/2$ is larger (in absolute value) than the one when $r < r_t$. Thus the magnetization increases and therefore r_t moves to the left.

(7.6) has been derived in [12] from the spin dynamics on a torus when the initial profile $m_0(r)$ has values in $(m^*, 1)$ for all r or when it has values in $(-1, -m^*)$. The result does not apply in the case of the Stefan problem where there are both positive and negative values of the magnetization: the derivation of the Stefan problem for Ising spins with Kawasaki dynamics and Kac potential is still an open problem.

8 Boundary layers, the bump

When $m_+ < m_\beta$ we get a completely different picture. Compare in fact the simulations in Fig. 8 and Fig. 9 where the initial state is the same but m_+ is stable in the former ($m_+ = 1$) and metastable ($m_+ = 0.93$) in the latter. In both cases, after a transient, we see a profile with a sharp (instanton-like) transition from $-m_\beta$ to $+m_\beta$ and then approximately linear

profiles which connect m_- to $-m_\beta$ and m_β to m_+. But, in the stable case the instanton-like region moves towards the center, while in the metastable case it moves towards 0 which is eventually reached. The same [heuristic] argument which explained in the case of Fig. 8 the motion of the instanton towards the center, now explains its motion away from the center: since $m_+ < m_\beta$ the slope of the pattern from the endpoint to the instanton is negative in the case of Fig. 9 (as it connects m_- to $-m_\beta$ and m_β to m_+); consequently the current in the interval from m_- to $-m_\beta$ is positive and larger than the one from m_β to m_+ (as the instanton in Fig. 9 is closer to 0 than to ℓ), thus the total magnetization increases and the instanton moves further towards 0.

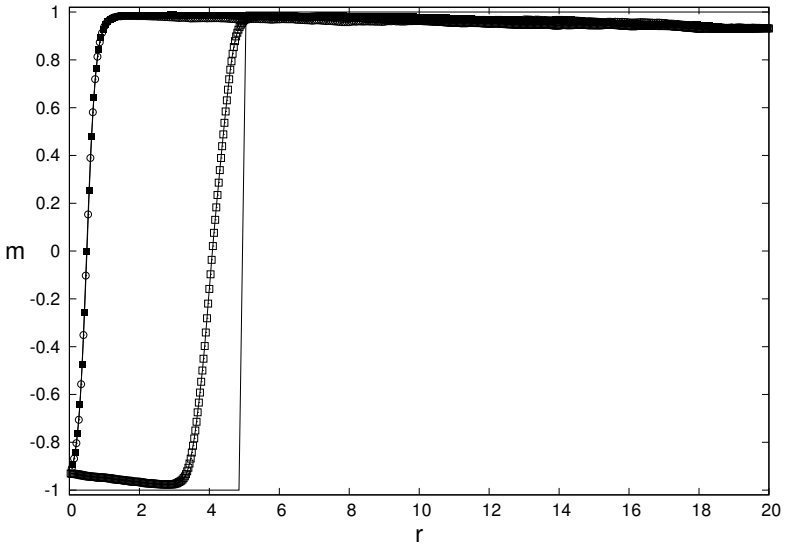

Figure 9: Magnetization profile with $m_+ = 0.93$. The different curves in the plot correspond to the averaged magnetization computed at different times: $t = 10^5$ (empty squares), $t = 10^6$ (black squares) and $t = 10^8$ (empty circles). The black thin line denotes the initial configuration, corresponding to a step function centered at $r = 5$.

The transition region in the stable case is approximated by an instanton which is a stationary solution of the evolution equations on the whole line. Analogously, when $m_+ < m_\beta$ we speculate that the transition region is approximated by a bump which is again a stationary solution $m(r)$, $r \geq 0$, of (5.6) on the half line with zero current and given boundary condition at 0, say μ, namely:

$$m(r) = \tanh\Big\{\beta[J * m(r) + h]\Big\}, \quad r \geq 0 \tag{8.8}$$

$$h = -J * m(0) + \frac{1}{\beta}\tanh^{-1}\mu, \qquad m(r) = \mu \text{ for } r < 0 \tag{8.9}$$

Indeed it can be easily seen that a stationary solution of (5.6) with zero current is necessarily a solution of (8.8). The Gibbsian formula (in the mesoscopic limit) would give (8.8) with $h = 0$, thus the problem (8.8) is not in the framework of the equilibrium theory. This is reflected by the appearance of an auxiliary magnetic field which has to be determined consistently with the magnetization pattern (as in the FitzHugh Nagumo models of the introduction where however by a mean field assumption the magnetization was simply a real number).

Observe that if $m(r)$ solves (8.8) with boundary condition μ then $-m(r)$ solves (8.8) with boundary condition $-\mu$, this symmetry will play an important role in the sequel. Besides the trivial solution $m(r) \equiv \mu$, existence of other solutions of (8.8) is an open problem. The simulations indicate the existence of increasing solutions, we thus define:

Definition. *The bump $B_\mu(r)$, $\mu \in (-m_\beta, m^*)$, is a non constant solution of* (8.8) *which is monotone non decreasing, We call $b(\mu)$ its asymptotic value:*

$$\lim_{r\to\infty} B_\mu(r) =: b(\mu) \tag{8.10}$$

Analogously we call B^-_μ, $m \in (-m^*, m_\beta)$ a non constant solution which is monotonic non increasing and denote by b^-_μ its asymptotic value. The existence B_μ implies the existence of B^-_μ, in fact by simmetry $B^-_\mu = -B_{-\mu}$. Thus what we will say for B_μ extends to B^-_μ and in the sequel we will consider only B_μ.

As mentioned above the existence of bumps is an open problem, the simulations indicate that bumps do indeed exist. The relation between bump and instanton can be understood in the following way. Call $\bar x(\mu)$ the value of r such that $\bar m(r) = \mu$. Replace the boundary condition $m(r) = \mu$, $r < 0$, in the definition of the bump by $m(r) = \bar m(r + \bar x(\mu))$, $r < 0$. Then the solution of (5.6) would be $m(r) = \bar m(r+\bar x(\mu))$, $r > 0$, with $h = 0$, the asymptotic value at $r = +\infty$ being m_β. Replacing $m(r) = \mu$ by $m(r) = \bar m(r + \bar x(\mu))$ for $r < 0$ is a small error if μ is close to $-m_\beta$ (because the instanton converges exponentially to its asymptotic values). One may then hope to prove in such a case the existence of the bump using perturbative techniques as in [7]–[8]. This has been done successfully in [8] for the equation

$$m(r) = \tanh\{\beta[J^{\rm neum} * m(r) + h]\}, \quad r \geq 0$$

where $J^{\rm neum}$ is defined with Neumann conditions; h above is fixed and sufficiently small.

We have numerical evidence of the existence of bumps. We have simulated (8.8) by looking at its discrete version with $\gamma^{-1} = 120$, $\ell = 5$ and Neumann conditions at the right boundary. We have solved such an equation by iteration: we start with $m \equiv 1$, compute h via (8.9) with such m and then define the first iterate m_1 as $m_1 = \tanh \beta(J * m + h)$. We then repeat the procedure till we find a fixed point. This is indeed reached (approximately) after a few iterations (in fact, three iterations already suffice to obtain good numerical convergence), see Fig. 10.

The numerical values of $b(\mu)$ are reported in Fig. 11, the main features are:

- the values of $b(\mu)$ are all in the metastable region,
- $b(m_+) = m_+$ if $m_+ \in (m^*, m_\beta)$, i.e. in the plus metastable region (left panel)
- $b(m_-) > b(m_+)$ for $m_- \in (-m_\beta, 0)$ and $m_+ = -m_-$ (right panel).

Conjecture *The bump B_μ exists for all $\mu < m^*$, when $\mu \in [m^*, m_\beta)$ there is no bump and we call $b(\mu) = \mu$. When $m_+ < m_\beta$ for all ℓ large enough there is a stationary solution $m_{\rm st}(r; \ell; m_\pm)$ of* (5.6)*, such that*

$$\lim_{\ell\to\infty} m_{\rm st}(r\ell; \ell; m_\pm) = m_{\rm st}(r; m_\pm), \quad r \in (0, 1) \tag{8.11}$$

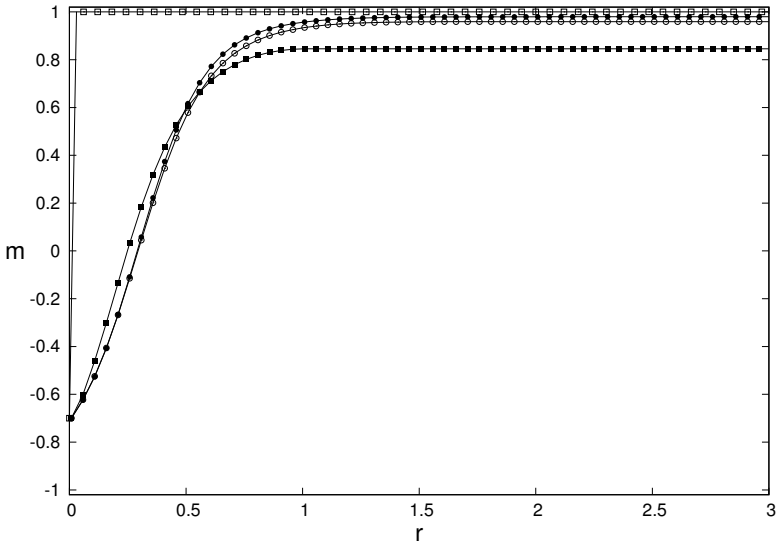

Figure 10: Iterations of Eq. (8.8), with $\beta = 2.5$, $\gamma^{-1} = 120$, $\ell = 5$ and $\mu = -0.7$. The different points denote, respectively, the initial condition (empty squares), the first iteration (black squares), the second iteration (empty circles) and the third iteration (black circles).

$$m_{\rm st}(0; m_\pm) = b(m_-), \quad m_{\rm st}(1; m_\pm) = b(m_+) \tag{8.12}$$

and

$$-\frac{1}{2}[1 - \beta(1 - m_{\rm st}^2)]\frac{dm_{\rm st}}{dr} = I_{\rm st}(m_+), \quad r \in [0, 1] \tag{8.13}$$

Remark. *Under the above Conjecture the channel has a positive current if*

$$b(\mu) > -\mu,\ \mu \in (-m_\beta, -m^*); \quad b(\mu) > b(-\mu),\ \mu \in (-m^*, 0) \tag{8.14}$$

As shown in the right panel of Fig. 11 there is clear numerical evidence of the validity of (8.14).

The equation (8.13) with boundary conditions (8.12) can be easily solved analytically thus determining $I_{\rm st}(m_+)$. By using the numerical values obtained for $b(m_-)$ and $b(m_+)$ we get the graph shown with empty circles in Fig. 12, where however $I_{\rm st}$ is divided by L in order to compare it with the experimental value $j(m_+)$ (black circle in Fig. 12) as given in Fig. 2. The agreement is good except in the interval $m_+ \in (m', m''')$, such a discrepancy will be discussed in the next section.

9 Stability of the bump

The numerical analysis of (8.8) suggests the following:

- there exists a bump solution B_μ for all $\mu \in (-m_\beta, m^*)$,
- when $\mu \in (-m_\beta, -m^*)$ there are two solutions: $m(x) \equiv \mu$ and $m(x) = B_\mu(x)$,

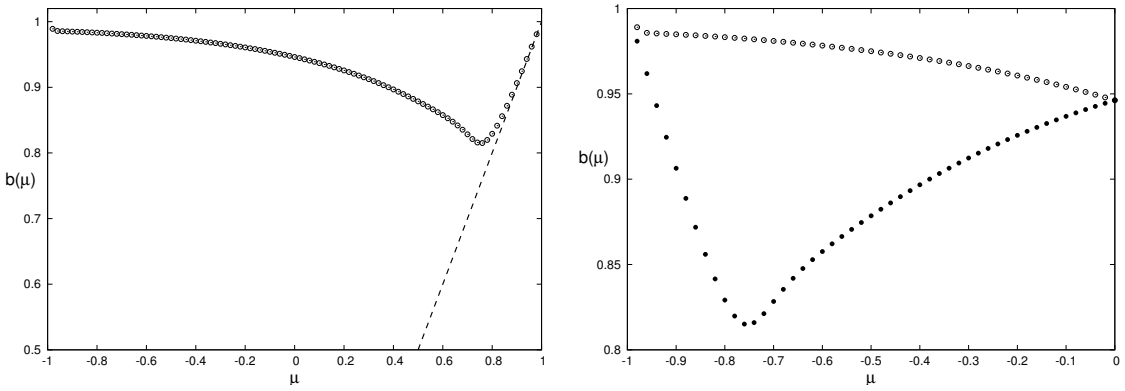

Figure 11: *Left panel*: Behavior of $b(\mu)$, with $\beta = 2.5$ and $\gamma^{-1} = 120$. The black dashed line denotes the curve $b(\mu) = \mu$. *Right panel*: For any $\mu \in (-m_\beta, 0)$ we report with an empty circle the value of $b(m_-)$ and with a black circles the value of $b(m_+)$, $m_+ = -m_-$.

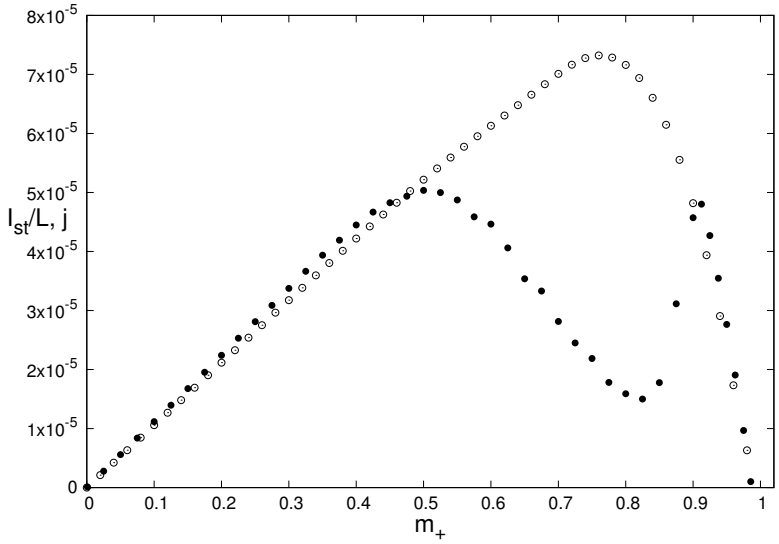

Figure 12: We plot $I_{\rm st}/L$ (empty circles) and $j := j^T_{{\rm ch}\to\mathcal{R}_2}$ (black circles) as functions of m_+ .

- when $\mu \in (-m^*, 0)$ there are three solutions: $m(x) \equiv \mu$, $m(x) = B_\mu(x)$ and $m(x) = -B_{-\mu}(x)$,

An alternative way to study the existence of the bump is by running the OS-CA with boundary conditions μ on the left and Neumann on the right. We take the same parameters $\gamma^{-1} = 120$ and $\ell = 5$ used for the numerical analysis of the solutions of (8.8) and start with an initial condition where all sites in the channel are occupied. Referring to Fig. 2, when $\mu \in (-m_\beta, m')$ we see, after a transient, a steady pattern close to B_μ. When $\mu \in (m^{\rm iv}, m_\beta)$ we see, after a transient, a steady pattern close to $m(x) \equiv \mu$. When $\mu \in (m', m^{\rm iv})$ the final pattern is close to $-B_{-\mu}$, see Fig. 13. Observe that the OS-CA does not select the bump solution when $\mu \in (m', m^{\rm iv})$ which is approximately the region where there is discrepancy between the theoretical and the experimental curves in Fig 12. We conjecture that this is due to γ being not small enough so we are far from the mesoscopic regime and stochastic fluctuations are relevant. Stochastic fluctuations may

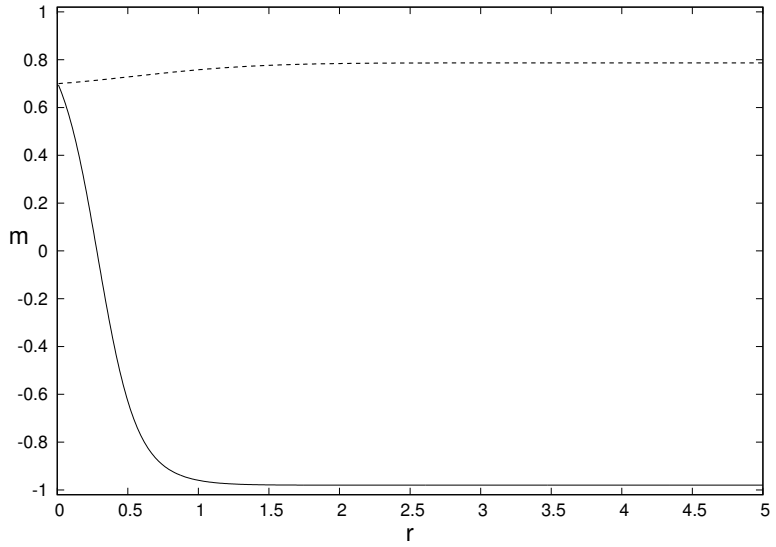

Figure 13: $\beta = 2.5$, $\gamma^{-1} = 120$, $\ell = 5$ and $\mu = 0.7 \in (m^{\rm iv}, m'')$. The black dashed line represents B_μ, the black thin line represents the asymptotic pattern of the CA which is close to $-B_{-\mu}$.

then determine tunnelling from the bump to patterns where there is a bump on the left and a minus bump on the right with an instanton in between them and patterns where the two bumps are both up. Indeed we have numerical evidence of all that, in the times of the simulations we see in fact the magnetization patterns oscillate as described above, see Fig.14.

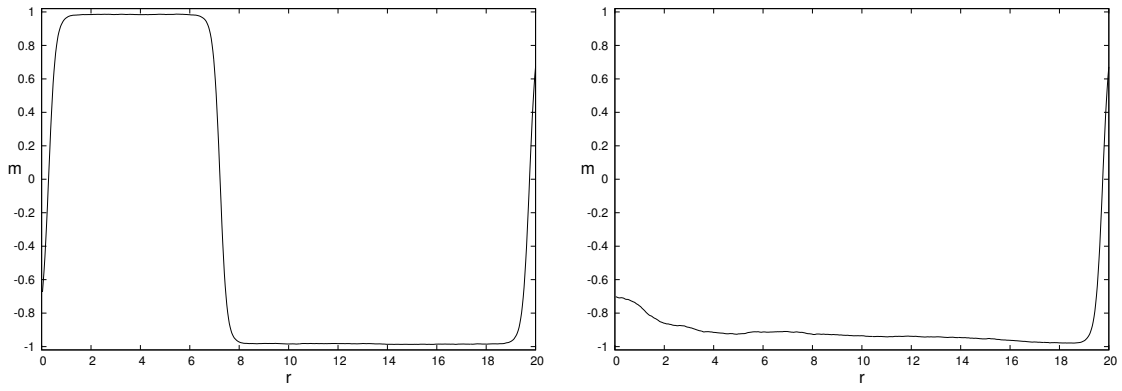

Figure 14: Typical (average) magnetization profile obtained at the beginning of a cycle (left panel) and at the end of a cycle (right panel).

10 Conclusions

We have presented two sets of simulations: the first one, see Fig. 6, shows that in the CC-CA there is a non zero current $j^{CC}(\gamma p)$ (provided the rate γp of exchanges between reservoirs is in some non zero interval); the second set of simulations, see Fig. 2, refers to

the OS-CA at magnetization $m_+ = -m_- > 0$ and shows that when $m_+ \in (0, m_\beta)$ then the current $j(m_+)$ goes "in the wrong direction", namely from the reservoir with m_- to that with m_+. We have a heuristic proof that what seen in Fig. 6 follows from the behavior of the channel in the OS-CA, as shown in Fig. 2; the proof relies on the validity of the mesoscopic and the adiabatic limits.

In the case of Fig. 2 the current is negative when $m_+ > m_\beta$ and positive when $m_+ < m_\beta$, in the former case the magnetization pattern in the channel shows the coexistence of the plus and minus phases while in the latter case only one phase appears (the statement in both cases refers to what happens in most of the volume). When the current is negative the values of the magnetization in the plus phase are larger than m_β and smaller than $-m_\beta$ in the negative one. Instead when the current is positive we are in the one phase regime and the values of the magnetization are metastable (thus there is a state with positive current which in the bulk takes positive metastable values and another state also with positive current which in the bulk takes negative metastable values). When the current is negative the plus and minus phases are connected via an instanton-like profile around the center of the channel, when the current is negative the unstable values of the magnetization are localized in a small region close to the endpoints. We thus have a boundary layer which leads quite abruptly from the imposed values of the magnetization at the boundaries to some metastable value after which the magnetization pattern is smooth and the current flows opposite to the magnetization gradient in agreement with the Fourier law.

The strange phenomenon of the current going "in the wrong direction" depends on the fact that the magnetization-jump in the boundary layer is more pronounced if it starts from lower values of the magnetization. Such a property, see (8.14), follows from the solution (the bump) of a non local equation describing the boundary layer, but its solution is obtained only numerically and we do not have a mathematical proof or even a heuristic explanation of why (8.14) should hold.

We expect that also in the Cahn-Hilliard equation the graph of $j(m_+)$ has a qualitatively similar shape as in Fig. 2, but we miss a proof.

We imagine that our results extend to more general systems with Kac potentials and maybe to physical systems where a van der Waals type of phase transition is present. In such cases a metastable interval is well defined and the relevant density (or magnetization) patterns in the bulk of the channel should have metastable values. Also for short range interactions, as in the n.n. Ising model with ferromagnetic interactions there are metastable values but the metastable region depends on the size of the system and shrinks to 0 as the volume diverges. Take the 2D Ising model in a squared box of side L: in the periodic case for β large it is proved that if $\pm m_\beta$ are the equilibrium magnetizations then for the canonical Gibbs measure with average magnetization $m \in (-m_\beta, -m_\beta + cL^{-2/3})$ and c small enough the phenomenon of phase separation is absent. Consider the Kawasaki dynamics at such values of β with periodic conditions on the horizontal sides of the box and exchanges of the spins in the vertical ones with infinite reservoirs at magnetization m_- and m_+ on the left and right. If what we have observed extends to this 2D Ising model we should see in the bulk magnetization patterns in the metastable phase, hence with values in an interval of size $L^{-2/3}$. The current should therefore scale as $L^{-1}L^{-2/3} = L^{-5/3}$ and if the boundary layer goes like in our case then the current would go from the small to the large values of the reservoirs magnetization.

A Estimates on the current between reservoirs

Recalling (2.9) we have

$$j_{\mathcal{R}_2\to\mathcal{R}_1}(t) = j_t := \zeta_t \sum_{i_+,i_-} \mathbf{1}_{\xi_t=(i_+,i_-)}[\theta''_t(i_+) - \theta''_t(i_-)] \tag{A.1}$$

where ζ_t and ξ_t are random variables independent of the process till time t and of θ''_t, they are also independent of each other. ζ_t takes value 1 with probability γp and value 0 with probability $1-\gamma p$; the values of ξ_t are pairs (i_+, i_-), $i_+ \in \mathcal{R}_2$, $i_- \in \mathcal{R}_1$ and $P(\xi_t = (i_+, i_-)) = \frac{1}{R^2}$. The sum $\sum_{i_+,i_-}$ is over $i_+ \in \mathcal{R}_2$ and $i_- \in \mathcal{R}_1$. We first estimate the expected value of $j_{\mathcal{R}_2\to\mathcal{R}_1}(t)$:

$$E_\gamma[j_{\mathcal{R}_2\to\mathcal{R}_1}(t)] = E_\gamma[\frac{N''_{\mathcal{R}_2}(t) - N''_{\mathcal{R}_1}(t)}{R}]\gamma p \tag{A.2}$$

where

$$N''_{\mathcal{R}_i}(t) = \sum_{i\in\mathcal{R}_i} \theta''_t(i), \quad i = 1, 2 \tag{A.3}$$

Since $|N''_{\mathcal{R}_i}(t) - N_{\mathcal{R}_i}(t)| \le 2$ for all t we have

$$\Big|E_\gamma[j_{\mathcal{R}_2\to\mathcal{R}_1}(t)] - \gamma p E_\gamma[\frac{N_{\mathcal{R}_2}(t) - N_{\mathcal{R}_1}(t)}{R}]\Big| \le \gamma p \frac{4}{R} \tag{A.4}$$

We will next prove (4.1). Since θ'' has values 0, 1 we have from (A.1)

$$E[j_t] \le \gamma p \tag{A.5}$$

By (2.5) the left hand site of (4.1), can be written as

$$A_T := E\Big[\{\frac{1}{T}\sum_{t=0}^{T-1}[j_t - \gamma p R^{-1}(N_{+,t} - N_{-,t})]\}^2\Big] \tag{A.6}$$

where

$$N_{+,t} = \sum_{i_+} \eta_t(i_+) = N_{\mathcal{R}_2}(t), \quad N_{-,t} = \sum_{i_-} \eta_t(i_-) = N_{\mathcal{R}_1}(t) \tag{A.7}$$

Define $N''_{\pm,t}$ as in (A.7) but with θ''_t instead of η_t and A''_T as in (A.6) but with $N''_{\pm,t}$.

Lemma 1.

$$A_T \le A''_T + \frac{16}{R}(\gamma p)^2 + \frac{16}{R^2}(\gamma p)^2 \tag{A.8}$$

Proof. Call

$$a_t = j_t - \gamma p R^{-1}(N''_{+,t} - N''_{-,t}) \tag{A.9}$$

$$b_t = \gamma p R^{-1}\{(N''_{+,t} - N''_{-,t}) - (N_{+,t} - N_{-,t})\} \tag{A.10}$$

Then

$$A_T = E\Big[\frac{1}{T^2}\sum_{s,t}(a_t - b_t)(a_s - b_s)\Big] \tag{A.11}$$

Hence

$$A_T \le A''_T + 2E\Big[\frac{1}{T^2}\sum_{s,t}|a_t||b_s|\Big] + E\Big[\frac{1}{T^2}\sum_{s,t}|b_s||b_t|\Big] \tag{A.12}$$

$|b_t| \le \gamma p \frac{4}{R}$ because $|N''_{+,t} - N''_{-,t}| \le R$ and $|N''_{\pm,t} - N_{\pm,t}| \le 2$. By (A.5) and $|N''_{+,t} - N''_{-,t}| \le R$ we get $E_\gamma[|a_t|] \le 2\gamma p$, therefore

$$A_T \le A''_T + 2\gamma p \frac{8}{R}\gamma p + [\gamma p \frac{4}{R}]^2 \tag{A.13}$$

□

Lemma 2. *Let $s < t$ and a_t as in* (A.9) *then*

$$E\Big[a_s a_t\Big] = 0 \tag{A.14}$$

Proof. By the independence properties of ζ_t and ξ_t:

$$E[a_s j_t] = E\Big[a_s \gamma p \sum_{i_+,i_-} R^{-2}[\theta''_t(i_+) - \theta''_t(i_-)]\Big] = E\Big[a_s \gamma p R^{-1}[N''_{+,t} - N''_{-,t}]\Big] \tag{A.15}$$

□

As a consequence

$$A''_T = \frac{1}{T^2}\sum_{t=0}^{T-1} E[a_t^2] \tag{A.16}$$

We expand the square in $E[a_t^2]$, the first term is

$$E\Big[\zeta_t \sum_{i_+,i_-}\sum_{i'_+,i'_-} \mathbf{1}_{\xi_t=(i_+,i_-)}\mathbf{1}_{\xi_t=(i'_+,i'_-)}[\theta''_t(i_+) - \theta''_t(i_-)][\theta''_t(i'_+) - \theta''_t(i'_-)]\Big]$$

Due to the characteristic functions $i_\pm = i'_\pm$ so that the above is bounded by γp. The double product in the expansion of $E[a_t^2]$ is bounded by $2(\gamma p)^2$ and the third term by $(\gamma p)^2$, so that

$$A''_T \le \frac{1}{T}\{\gamma p + 3(\gamma p)^2\} \tag{A.17}$$

Going back to (A.13) we get

$$A_T \le \frac{1}{T}\{\gamma p + 3(\gamma p)^2\} + 16\frac{(\gamma p)^2}{R} + 16[\frac{\gamma p}{R}]^2 \tag{A.18}$$

which concludes the proof of (4.1).

B Proof of Theorems 1 and 2

Proof of (5.6)**.** Here we prove that $m(r,t)$ satisfies (5.6) both in the CC-CA and in the OS-CA.

Let $u(r,t) = m(r,t) + 1$ then m satisfies (5.6) if and only if u satisfies

$$\frac{\partial}{\partial t}u(r,t) = \frac{1}{2}\frac{\partial^2 u}{\partial r^2} - C\frac{\partial}{\partial r}\Big\{[u(2-u]\int_r^{r+1}[u(r+\xi,t) - u(r-\xi,t)]d\xi\Big\} \quad \text{(B.1)}$$

with $u(r+\xi,t) = u_+(t) = m_+(t) + 1$ if $r + \xi \geq \ell$ and $u(r-\xi,t) = u_-(t) = m_-(t) + 1$ if $r - \xi \leq 0$. In the OS-CA $m_\pm(t) \equiv m_\pm$.

By (5.2)

$$\begin{aligned} &\lim_{\gamma\to 0}\lim_{\gamma x\to r,\gamma^2 t\to\tau} E_\gamma[\eta(x,v,t)] = \frac{1}{2}u(x,t), \qquad v \in \{-1,1\} \\ &\lim_{\gamma\to 0}\lim_{\gamma x\to r,\gamma^2 t\to\tau} u_\gamma(x,t) = u(x,t), \qquad u_\gamma(x,t) = E_\gamma[\eta(x,t)] \end{aligned} \quad \text{(B.2)}$$

So that we need to prove that the limit of u_γ satisfies (B.1).

By assumpotion $u(r,t)$ is smooth so that it is enough to prove weak convergence namely that for any smooth test function $f(r,t)$ with compact support in $(0,\ell)\times(0,\infty)$,

$$\begin{aligned} \int u(r,t)\frac{\partial f(r,t)}{\partial t}drdt &= -\frac{1}{2}\int u(r,t)\frac{\partial^2 f(r,t)}{\partial r^2}drdt \\ &- \int \frac{\partial f(r,t)}{\partial r}C\Big\{[u(2-u]\int_r^{r+1}[u(r+\xi,t) - u(r-\xi,t)]\Big\}drdt \end{aligned} \quad \text{(B.3)}$$

By an integration by parts

$$\int u(r,t)\frac{\partial f(r,t)}{\partial t}drdt = -\lim_{\gamma\to 0}\gamma^3\sum_{x,t} f(\gamma x,\gamma^2 t)\gamma^{-2}\{u_\gamma(x;t+1) - u_\gamma(x;t)\}$$

We will next consider $u_\gamma(x;t+1) - u_\gamma(x;t)$. Recalling that $j_{x,x+1}(t)$ is the number of particles which in the time step $t, t+1$ cross the bond $(x,x+1)$, $x \in \{1,..,L-1\}$ (counting as positive those which jump from x to $x+1$ and as negative those from $x+1$ to x), we have

$$u_\gamma(x;t+1) - u_\gamma(x;t) = E_\gamma[j_{x-1,x}(t)] - E_\gamma[j_{x,x+1}(t)]$$

We then have denoting by ∇_γ the discrete derivative ($\nabla_\gamma\varphi(x) = \varphi(x+1) - \varphi(x)$),

$$\int u(r,t)\frac{\partial f(r,t)}{\partial t}drdt = -\lim_{\gamma\to 0}\gamma^3\sum_{x,t}\gamma^{-1}\nabla_\gamma f(\gamma x,\gamma^2 t)\gamma^{-1}E_\gamma[j_{x,x+1}(t)] \quad \text{(B.4)}$$

Lemma 3.

$$E_\gamma[j_{x,x+1}(t)] = \frac{1}{2}[u_\gamma(x;t) - u_\gamma(x+1;t) + E_\gamma\Big[\chi_{x,\gamma;t}\epsilon_{x,\gamma;t} + \chi_{x+1,\gamma;s}\epsilon_{x+1,\gamma;t}\Big] \quad \text{(B.5)}$$

where $\epsilon_{x,\gamma;t}$ is $\epsilon_{x,\gamma}$ computed at time t and

$$\chi_{x,\gamma;t} = \eta(x,1;t)\Big(1-\eta(x,-1;t)\Big) + \eta(x,-1;t)\Big(1-\eta(x,1;t)\Big)$$

Proof. Observe that the expected number of particles that goes from x to $x+1$ is

$$E_\gamma\Big[\eta(x,1;t)\eta(x,-1,t) + \chi_{x,\gamma;t}(\frac{1}{2} + \epsilon_{x,\gamma;t})\Big] = \frac{1}{2}u_\gamma(x,t) + E_\gamma\Big[\chi_{x,\gamma;t}\epsilon_{x,\gamma;t}\Big]$$

The expected number of particles that goes from $x+1$ to x is

$$E_\gamma\big[\eta(x+1,1;t)\eta(x+1,-1,t)+\chi_{x+1,\gamma;t}(\frac{1}{2}-\epsilon_{x+1,\gamma;t})\big]=\frac{1}{2}u_\gamma(x+1,t) \\ -E_\gamma\big[\chi_{x+1,\gamma;t}\epsilon_{x+1,\gamma;t}\big]$$

so that we get (B.5). □

We insert (B.5) in (B.4) and, denoting by Δ_γ the discrete laplacian, we get

$$\gamma^3\sum_{x,t}\gamma^{-1}\nabla_\gamma f(\gamma x,\gamma^2 t)\gamma^{-1}j_\gamma(x,x+1,t)=\frac{1}{2}\gamma^3\sum_{x,t}\gamma^{-2}\Delta_\gamma f(\gamma x,\gamma^2 t)u_\gamma(x,t) \\ +\gamma^3\sum_{x,t}\gamma^{-1}2f'(\gamma x,\gamma^2 t)E_\gamma[\chi_{x,\gamma;t}]E_\gamma[\gamma^{-1}\epsilon_{x,\gamma;t}]+R_\gamma \tag{B.6}$$

where $2f'(\gamma x,\gamma^2 t)=[\nabla_\gamma f(\gamma x,\gamma^2 t)+\nabla_\gamma f(\gamma(x-1),\gamma^2 t)]$ and

$$R_\gamma:=2\gamma^3\sum_{x,t}\gamma^{-1}2f'(\gamma x,\gamma^2 t)E_\gamma[\chi_{x,\gamma;t}\Big(\gamma^{-1}\epsilon_{x,\gamma;t}-E_\gamma[\gamma^{-1}\epsilon_{x,\gamma;t}]\Big)]$$

By (B.3) and (5.4)

$$\lim_{\gamma\to 0}\lim_{\gamma x\to r,\gamma^2 t\to\tau}E_\gamma[\chi_{x,\gamma;t}]=\frac{1}{2}u(r,t)[2-u(r,t)] \\ \lim_{\gamma\to 0}\lim_{\gamma x\to r,\gamma^2 t\to\tau}E_\gamma[\gamma^{-1}\epsilon_{x,\gamma;t}]=\int_r^{r+1}C[u(r+\xi,t)-u(r-\xi,t)]d\xi \tag{B.7}$$

We postpone the proof of

$$\lim_{\gamma\to 0}\gamma^3\sum_{x=2}^{\gamma^{-1}\ell-1}\sum_{t=1}^{\gamma^{-2}T}E_\gamma\Big[\big|\gamma^{-1}\epsilon_{x,\gamma;t}-E_\gamma[\gamma^{-1}\epsilon_{x,\gamma;t}]\big|\Big]=0 \tag{B.8}$$

where $(0,\ell)\times(0,T)$ contains the support of $f(r,t)$.
Observe that (B.4), (B.6), (B.7) and (B.8) yield (B.3) concluding the proof of □

Proof of (B.8)**.** By Cauchy-Schwartz it is enough to prove that

$$\lim_{\gamma\to 0}\gamma^3\sum_{x=2}^{\gamma^{-1}\ell-1}\sum_{t=1}^{\gamma^{-2}T}E_\gamma\Big[\big|\gamma^{-1}\epsilon_{x,\gamma;t}-E_\gamma[\gamma^{-1}\epsilon_{x,\gamma;t}]\big|^2\Big]=0 \tag{B.9}$$

We thus need to compute the limit of

$$\gamma^5\sum_{r,r',r''\in\gamma\mathbb{Z}}\sum_{\tau\in\gamma^2\mathbb{Z}}g_\gamma(r,r',r'',\tau) \tag{B.10}$$

where $\gamma^{-1}r\in[2,\gamma^{-1}\ell-1]$, $|r'-r|\le 1$, $|r''-r|\le 1$, $\gamma^{-2}\tau\in[1,\gamma^{-2}T]$ and

$$g_\gamma(r,r',r'',\tau)=C^2E_\gamma[\tilde\eta_{\gamma^{-2}\tau}(\gamma^{-1}(r'-r))\tilde\eta_{\gamma^{-2}\tau}(\gamma^{-1}(r''-r))] \tag{B.11}$$

where $\tilde\eta_t(x) = \eta(x,t) - E_\gamma[\eta(x,t)]$ if $x \in [1,L]$, otherwise it is $= \frac{2N_{\mathcal{R}_i}}{R} - E_\gamma[\frac{2N_{\mathcal{R}_i}}{R}]$ where $i=2$ if $x > L$ and $i=1$ if $x<1$ otherwise in the OS-CA is equal to $m_\pm$ respectively. By (5.4) and (5.5), (B.10) vanishes as $\gamma \to 0$. □

Proof of (5.11)**.** We call

$$I^T_{x,\gamma} = \gamma \sum_{t=0}^{T-1} E_\gamma[j_{x,x+1}(t)] \tag{B.12}$$

Lemma 4. *There are c and c' so that for all $r' < r''$ in $(0,\ell)$*

$$\Big|\frac{1}{x''-x'}\sum_{y=x'}^{x''} I^T_{y,\gamma}\Big| \le c, \qquad x' = [\gamma^{-1}r'], \quad x'' = [\gamma^{-1}r''] \tag{B.13}$$

$$\Big|I^T_{x'',\gamma} - I^T_{x',\gamma}\Big| \le c'|r''-r'| \tag{B.14}$$

Proof. By (B.5), using that $|\chi_{x,\gamma;t}| \le 2$ and $|\epsilon_{x,\gamma;t}| \le 2C\gamma$ for all x and t and after telescopic cancellations we get

$$\Big|\frac{1}{x''-x'}\sum_{y=x'}^{x''} I^T_{y,\gamma}\Big| \le \big|\gamma \sum_{s=0}^{T-1} \frac{1}{x''-x'} E_\gamma[\frac{1}{2}(\eta(x',s) - \eta(x''+1,s))]\big| + 8C\gamma^2 T$$

The right hand side converges to $\frac{1}{r''-r'}\int_0^\tau \frac{1}{2}[m(r'.s) - m(r'',s)]ds + 8C^2\tau$ which, by the smoothness of m, proves (B.13).

We have that

$$\Big|\gamma\sum_{t=0}^{T-1} j_{x',x'+1}(t)] - \gamma\sum_{t=0}^{T-1} j_{x'',x''+1}(t)\Big| \le c'\gamma|x''-x'|$$

because the particles which contribute to the left hand site are: (1) those which reach for the first time $x'+1$ jumping from x' and at the final time are in $[x'+1, x'']$; (2) those which reach for the first time x'' jumping from $x''+1$ and at the final time are in $[x'+1, x'']$; (3) those initially in $[x'+1, x'']$ and which leave this interval for the last time jumping to $x''+1$; (4) those initially in $[x'+1, x'']$ and which leave this interval for the last time jumping to x'. □

The family $\{I^T_{x,\gamma}\}$ thought as functions of $r = \gamma x$ are equibounded and equicontinuous in any compact of $(0,\ell)$, thus they converge pointwise by subsequences. We will then prove (5.11) by identifying the limit. By continuity it will be enough to prove

$$\lim_{\gamma\to 0} \frac{1}{x''-x'}\sum_{y=x'}^{x''} I^T_{x,\gamma} = \frac{1}{r''-r'}\int_{r'}^{r''} dr \int_0^\tau I(r,s)ds \tag{B.15}$$

By (B.5)

$$\begin{aligned}\frac{1}{x''-x'}\sum_{y=x'}^{x''} I^T_{x,\gamma} &= \gamma\sum_{s=0}^{T-1}\Big\{\frac{1}{x''-x'}E_\gamma[\frac{1}{2}(\eta(x',s)-\eta(x''+1,s))] \\ &+ \frac{1}{x''-x'}\sum_{y=x'}^{x''} E_\gamma[\chi_{x,\gamma;s}\epsilon_{x,\gamma;s} + \chi_{x+1,\gamma;s}\epsilon_{x+1,\gamma;s}]\Big\}\end{aligned}$$

The first term converges to

$$\frac{1}{r''-r'}\frac{1}{2}\int_0^\tau [m(r',s)-m(r'',s)]ds = \frac{1}{r''-r'}\frac{1}{2}\int_0^\tau ds\int_{r'}^{r''} dr\frac{\partial m(r,s)}{\partial s} \tag{B.16}$$

By (B.7) and (B.8) the second one converges to

$$-\frac{1}{r''-r'}\int_0^\tau\int_{r'}^{r''} C[1-m^2]\int_r^{r+1}[m(r+\xi,s)-m(r-\xi,s)]d\xi dr ds$$

Proof of (5.12)**.** As the two are similar, we just prove the second equality in (5.12). The same proof as the one for (B.14) shows that

$$\left|I^T_{x,\gamma}-I^T_{\mathrm{ch}\to\mathcal{R}_2,\gamma}\right|\le c'|\ell-r|,\qquad x=[\gamma^{-1}r] \tag{B.17}$$

where

$$I^T_{\mathrm{ch}\to\mathcal{R}_2,\gamma}=\gamma\sum_{t=0}^{T-1}E_\gamma[j_{\mathrm{ch}\to\mathcal{R}_2}(t)]$$

Let $\tilde I$ be a limit point of $I^T_{\mathrm{ch}\to\mathcal{R}_2,\gamma}$ as $\gamma\to 0$ then

$$\Big|\int_0^\tau I(r,s)ds-\tilde I\Big|\le c'|\ell-r|$$

Using the expression (5.6) for $I(r,t)$ and the continuity of m, we get in the limit $r\to\ell$ that $\tilde I=\int_0^\tau I(\ell,s)ds$.

Proof of (5.8). As the proofs are similar, we just prove the second equality in (5.8) for the CC-CA. Suppose by contradiction that there is $t>0$ such that $m(\ell,t)\neq m_+(t)$ and for the sake of definiteness $m(\ell,t)<m_+(t)$. Then there is $\delta>0$ and an interval $[t',t'']$ so that for $s\in[t',t'']$, $m_+(t)>m(\ell,t)+\delta$. Recalling the proof of Lemma 3

$$\begin{aligned}E_\gamma[j_{\mathrm{ch}\to\mathcal{R}_2}(s)] &= E_\gamma[\frac{N_{\mathcal{R}_2}(s)}{R}]-\frac{1}{2}u_\gamma(L,s)-E_\gamma\Big[\chi_{L,\gamma;s}\epsilon_{L,\gamma;s}\Big]\\ &\ge E_\gamma[\frac{N_{\mathcal{R}_2}(s)}{R}]-\frac{1}{2}u_\gamma(L,s)-c\gamma\end{aligned}$$

c a suitable constant, $c\gamma$ bounding the term with $\epsilon_{x,\gamma}$. Then, recalling (2.3), (2.5), (2.6) and using the assumptions in Theorem 1 we get

$$\liminf_{\gamma\to0}\gamma^2\sum_{s\in\mathbb{Z}\cap\gamma^{-2}[t',t'']}E_\gamma[j_{\mathrm{ch}\to\mathcal{R}_2}(s)] \;\ge\; \frac{1}{2}\int_{t'}^{t''}[m_+(s)-m(\ell,s)]ds\ge\frac{\delta}{2}[t''-t']$$

which contradicts (5.12).

The dynamics of the reservoirs. We just prove (5.9). Let $\tau_0\ge0$, $\tau>0$, $t_0=[\gamma^{-2}\tau_0]$, $T=[\gamma^{-2}\tau]$, then

$$N_{\mathcal{R}_2}(t_0+T)-N_{\mathcal{R}_2}(t_0)=\sum_{t=t_0}^{t_0+T-1}\Big[j_{\mathrm{ch}\to\mathcal{R}_2}(t)-j_{\mathcal{R}_2\to\mathcal{R}_1}(t)\Big]$$

We take the expectation and we use (A.4) to get

$$\Big|E_\gamma[N_{\mathcal{R}_2}(t_0+T)-N_{\mathcal{R}_2}(t_0)]-\sum_{t=t_0}^{t_0+T-1}\Big[E_\gamma[j_{\mathrm{ch}\to\mathcal{R}_2}(t)]-E_\gamma[\frac{N_{\mathcal{R}_2}(t)-N_{\mathcal{R}_1}(t)}{R}]\gamma p\Big]\Big| \leq \frac{4\gamma p}{R}T \tag{B.18}$$

We then get

$$\frac{a}{2}[m_+(\tau_0+\tau)-m_+(\tau_0)]=\int_{\tau_0}^{\tau_0+\tau}I(\ell,s)ds-p\int_{\tau_0}^{\tau_0+\tau}\frac{1}{2}[m_+(s)-m_-(s)]ds \tag{B.19}$$

which is obtained from (B.18) by multiplying by γ and taking the limit $\gamma\to 0$ after using that (1) $R=a\gamma^{-1}$, (2) by (5.3)

$$\lim_{\gamma\to 0}E_\gamma[\frac{N_{\mathcal{R}_2}(t)-N_{\mathcal{R}_1}(t)}{R}]=\frac{m_+(\tau)-m_-(\tau)}{2},\quad t=[\gamma^{-2}\tau]$$

(3) by (5.12)

$$\lim_{\gamma\to 0}\gamma\sum_{t=t_0}^{t_0+T-1}E_\gamma[j_{\mathrm{ch}\to\mathcal{R}_2}(t)]=\int_{\tau_0}^{\tau_0+\tau}I(\ell,s)ds$$

Then (5.9) is obtained from (B.19) by dividing by τ and taking the limit $\tau\to 0$.

Acknowledgements The authors acknowledge very useful discussions with Dima Ioffe.

References

[1] P. Bruno, *Comment on "Quantum Time Crystals"*, Phys. Rev. Lett. **110**, 118901 (2013).

[2] L. A. Bunimovich, *Mushrooms and other billiards with divided phase space*, Chaos **11**, 802–808 (2001).

[3] M. Colangeli, A. De Masi, E. Presutti, *Latent heat and the Fourier law*, Physics Letters A **380**, 1710–1713 (2016).

[4] P. Dai Pra , M. Fischer, D. Regoli, *A Curie-Weiss Model with Dissipation*, Journal of Statistical Physics **152**, 37–53 (2013).

[5] A. De Masi, E. Presutti, D. Tsagkarogiannis, *Fourier law, phase transitions and the stationary Stefan problem*, Archive for Rational Mechanics and Analysis **201**, 681–725 (2011).

[6] A. De Masi, S. Olla, *Quasi-static hydrodynamic limit*, Journal of Statistical Physics **161**, 1037–1058 (2015).

[7] A. De Masi, E. Olivieri, E. Presutti, *Spectral properties of integral operators in problems of interface dynamics and metastability*, Markov Processes and Related Fields **4**, 27–112, (1998).

[8] A. De Masi, E. Olivieri, E. Presutti, *Critical droplet for a non local mean field equation*, Markov Processes and Related Fields **6**, 439–471 (2000).

[9] G. B. Giacomin, C. Poquet, *Noise, interaction, nonlinear dynamics and origin of rhythmic behaviors*, Brazilian Journal of Probability and Statistics **29**, 460–493 (2015).

[10] G.B. Giacomin, J. L. Lebowitz, *Phase segregation dynamics in particle systems with long range interactions. I. Macroscopic limits*, Journal of Statistical Physics **87**, 37–61 (1997).

[11] Y. Kuramoto, *Chemical oscillations, waves and turbulence*, Springer Series in Synergetics, Springer - Verlag Heidelberg (1984).

[12] J. L. Lebowitz, E. Orlandi, E. Presutti, *A particle model for spinodal decomposition*, Journal of Statistical Physics **63**, 933–974 (1991).

[13] J. L. Lebowitz, O. Penrose, *Rigorous Treatment of the Van Der Waals-Maxwell Theory of the Liquid-Vapor Transition*, Journal of Mathematical Physics **7**, 98–113 (1966).

[14] E. Presutti, *Scaling limits in statistical mechanics and microstructures in continuum mechanics* Springer, Theoretical and Mathematical Physics, Springer-Verlag Berlin Heidelberg (2009).

[15] P. A. Tass, *Phase resetting in Medicine and Biology: Stochastic Modelling and Data Analysis*, Springer Series in Synergetics, Springer-Verlag Berlin Heidelberg (1999).

[16] F. Wilczek, *Quantum time crystals.* Phys. Rev. Lett. **109**, 160401 (2012).

[17] A. Shapere, F. Wilczek, Classical time crystals, Phys. Rev. Lett. **109**, 160402 (2012).

[18] J. Zhang, P. W. Hess, A. Kyprianidis, P. Becker, A. Lee, J. Smith, G. Pagano, I.-D. Potirniche, A. C. Potter, A. Vishwanath, N. Y. Yao, C. Monroe, *Observation of a Discrete Time Crystal*. arXiv:1609.08684 (2016).